SIAM J. SCI. COMPUT.
Vol. 41, No. 6, pp. B1284–B1309

COMPUTING GROUND STATES OF BOSE–EINSTEIN CONDENSATES WITH HIGHER ORDER INTERACTION VIA A REGULARIZED DENSITY FUNCTION FORMULATION*

WEIZHU BAO† AND XINRAN RUAN‡

Abstract. We propose and analyze a new numerical method for computing the ground state of the modified Gross–Pitaevskii equation for modeling the Bose–Einstein condensate with a higher order interaction by adapting the density function formulation and the accelerated projected gradient method. By reformulating the energy functional $E(\phi)$ with ϕ, the wave function, in terms of the density $\rho = |\phi|^2$, the original nonconvex minimization problem for defining the ground state is then reformulated to a convex minimization problem. In order to overcome the semismoothness of the function $\sqrt{\rho}$ in the kinetic energy part, a regularization is introduced with a small parameter $0 < \varepsilon \ll 1$. Convergence of the regularization is established when $\varepsilon \to 0$. The regularized convex optimization problem is discretized by the second order finite difference method. The convergence rates in terms of the density and energy of the discretization are established. The accelerated projected gradient method is adapted for solving the discretized optimization problem. Numerical results are reported to demonstrate the efficiency and accuracy of the proposed numerical method. Our results show that the proposed method is much more efficient than the existing methods in the literature, especially in the strong interaction regime.

Key words. Bose–Einstein condensate, higher order interaction, ground state, density function formulation, accelerated projected gradient method

AMS subject classifications. 35Q55, 65N06, 65N25, 90C30

DOI. 10.1137/19M1240393

1. Introduction.

The Bose–Einstein condensate (BEC) has drawn great attention since its first experimental realization in 1995 [1, 15, 25] because of its huge potential value in exploring a wide range of questions in fundamental physics. Mathematically, a BEC can be effectively approximated via a Gross–Pitaevskii equation (GPE), which is a mean field model considering only the binary contact interaction of form [32, 33, 38]

$$V_{\rm int}(\mathbf{x}_1 - \mathbf{x}_2) = g_0 \delta(\mathbf{x}_1 - \mathbf{x}_2), \quad \mathbf{x}_1, \mathbf{x}_2 \in \mathbb{R}^3, \tag{1.1}$$

where $\delta(\cdot)$ is the Dirac delta function, $g_0 = \frac{4\pi\hbar^2 a_s}{m}$ is the contact interaction strength with a_s being the s-wave scattering length, $\hbar$ being the reduced Planck constant and m being the mass of the particle [33]. The great success of GPE comes from the fact that BEC is extremely dilute and the confinement is weak in most experiments. However, recent progress in experiments, such as the application of Feshbach resonances in cold atomic collision [21, 26, 39], enables us to tune the scattering length in a larger range. In such experiments, the underlying assumptions of the GPE and its validity have to be carefully examined. As shown in [23, 28, 45], a higher order interaction (HOI)

*Submitted to the journal's Computational Methods in Science and Engineering section January 23, 2019; accepted for publication (in revised form) September 4, 2019; published electronically November 19, 2019.

https://doi.org/10.1137/19M1240393

Funding: This work was supported by the Academic Research Fund of Ministry of Education of Singapore grant R-146-000-247-114.

†Department of Mathematics, National University of Singapore, Singapore 119076, Singapore (matbaowz@nus.edu.sg, http://blog.nus.edu.sg/matbwz/).

‡Sorbonne Université, CNRS, Université de Paris, Inria, Laboratoire J.-L. Lions, F-75005, Paris, France (xinran.ruan@sorbonne-universite.fr).

has to be included for a better description. With the HOI term, the new binary interaction takes the form [23, 28, 45]

$$\tilde{V}_{\rm int}(\mathbf{z}) = V_{\rm int}(\mathbf{z}) + V_{\rm HOI}(\mathbf{z}) = g_0\delta(\mathbf{z}) + g_0 g_1 \left(\delta(\mathbf{z})\nabla_{\mathbf{z}}^2 + \nabla_{\mathbf{z}}^2\delta(\mathbf{z})\right), \tag{1.2}$$

where $\mathbf{z} = \mathbf{x}_1 - \mathbf{x}_2 \in \mathbb{R}^3$, $\delta(\cdot)$ and g_0 are defined as before, and g_1, the strength of the HOI, is defined as $g_1 = \frac{a_s^2}{3} - \frac{a_s r_e}{2}$ with r_e being the effective range of the two-body interaction. With the new binary interaction (1.2), the dimensionless modified GPE (MGPE) in d-dimensions (d=1,2,3) can be derived as [23, 29, 30, 41, 42, 43]

$$i\partial_t\psi = \left[-\frac{1}{2}\Delta + V(\mathbf{x}) + \beta|\psi|^2 - \delta\Delta(|\psi|^2)\right]\psi, \quad t > 0, \quad \mathbf{x} \in \mathbb{R}^d, \tag{1.3}$$

where $\psi = \psi(\mathbf{x}, t)$ is the complex-valued wave function, $V(\mathbf{x}) \geq 0$ is the external potential, and the dimensionless parameters β and δ denote the contact interaction strength and the HOI strength, respectively. Define the energy to be

$$\tilde{E}(\psi(\cdot, t)) := \int_{\mathbb{R}^d} \left[\frac{1}{2}|\nabla\psi|^2 + V(\mathbf{x})|\psi|^2 + \frac{\beta}{2}|\psi|^4 + \frac{\delta}{2}|\nabla|\psi|^2|^2\right] d\mathbf{x}. \tag{1.4}$$

It is easy to check that the MGPE (1.3) conserves the *mass* (or *normalization*) [41] as

$$\|\psi(\cdot, t)\|_2^2 = \int_{\mathbb{R}^d} |\psi(\mathbf{x}, t)|^2\, d\mathbf{x} \equiv \int_{\mathbb{R}^d} |\psi(\mathbf{x}, 0)|^2\, d\mathbf{x} = \|\psi(\cdot, 0)\|_2^2 = 1, \tag{1.5}$$

and the *energy* (1.4) [41], i.e.,

$$\tilde{E}(\psi(\cdot, t)) \equiv \tilde{E}(\psi(\cdot, 0)), \quad t \geq 0. \tag{1.6}$$

To find the ground state of a BEC is a fundamental problem since the ground state represents the most stable stationary state of the system. Mathematically speaking, the ground state of a BEC described by the MGPE (1.3) is defined as the minimizer of the energy functional (1.4) under the normalization constraint (1.5). Specifically, we have the ground state $\phi_g = \phi_g(\mathbf{x})$ defined as [7, 41]

$$\phi_g := \arg\min_{\phi \in S} \tilde{E}(\phi), \tag{1.7}$$

where $S := \{\phi \,|\, \|\phi\|_2 = 1, \quad \tilde{E}(\phi) < \infty\}$. The corresponding energy $E_g := \tilde{E}(\phi_g)$ is called the ground state energy. The Euler–Lagrange equation of the problem (1.7) implies that the ground state ϕ_g satisfies the following nonlinear eigenvalue problem [7, 41]

$$\mu\phi = \left[-\frac{1}{2}\Delta + V(\mathbf{x}) + \beta|\phi|^2 - \delta\Delta(|\phi|^2)\right]\phi, \quad \mathbf{x} \in \mathbb{R}^d, \tag{1.8}$$

under the normalization constraint $\|\phi\|_2 = 1$, where μ is the corresponding chemical potential (or eigenvalue in mathematics) and can be computed as [7, 41]

$$\mu(\phi) = \tilde{E}(\phi) + \int_{\mathbb{R}^d} \left[\frac{\beta}{2}|\phi|^4 + \frac{\delta}{2}\left|\nabla|\phi|^2\right|^2\right] d\mathbf{x}. \tag{1.9}$$

The existence and uniqueness of the ground state of the nonconvex optimization problem (1.7) has been thoroughly studied in [7]. When $\delta = 0$, the MGPE (1.3) degenerates to a GPE and the existence and uniqueness of the ground state is clear. We refer readers to [5, 6, 38] and references therein. When $\delta \neq 0$, the ground state exists if and only if $\delta > 0$, and it can be chosen to be positive. Furthermore, the positive ground state is unique if we have both $\beta \geq 0$ and $\delta \geq 0$. Therefore, throughout the paper, we will only consider the special case where $\delta \geq 0$ and $\beta \geq 0$ for the numerical computation. In particular, we are interested in the Thomas–Fermi limit with a strong HOI effect, i.e., $\delta \gg 1$. The exact Thomas–Fermi limit of the ground state with strong repulsive interaction has been studied in details in [42].

In this paper, we aim to design a numerical method to compute the ground state defined in (1.7). When $\delta = 0$, the MGPE (1.3) degenerates to the classical GPE and numerous methods have been proposed for this special case, such as the normalized gradient flow method [3, 4, 10, 22, 8, 9], a Runge–Kutta spectral method with spectral discretization in space and Runge–Kutta-type integration in time [35], Gauss–Seidel-type methods [20], a finite element method by directly minimizing the energy functional [11], a regularized Newton method [44], a method based on Riemannian optimization [24], a preconditioned nonlinear conjugate gradient method [2]. However, to our best knowledge, there are few numerical schemes proposed for the case $\delta > 0$. The strong HOI effect, i.e., $\delta \gg 1$, introduces high nonlinearity, which may result in inefficiency and instability of the numerical methods proposed for the $\delta = 0$ case. For instance, the regularized Newton method would become extremely slow when δ is large, which will be shown later via numerical experiments, while the normalized gradient flow method could even fail as shown in [40], even if a convex-concave splitting of the HOI term is adapted to significantly improve the robustness of the method.

To resolve the problem, we propose in the paper a novel method, namely, the rDF-APG method, where the term "rDF-APG" means using the regularized density function formulation and accelerated projected gradient method for optimization. The method works by directly minimizing the energy functional formulated via the density function $\rho = |\phi|^2$ instead of the wave function ϕ. In fact, the idea of formulating the energy functional via the density function has been widely used in the Thomas–Fermi models [19, 34] and the density functional theory [18, 31], a most popular and versatile method in condensed-matter physics, computational physics, and computational chemistry. However, to our best knowledge, there are few works in adapting the density function formulation in designing efficient and accurate numerical methods for computing ground states and dynamics of BEC. With the density function formulation, although the kinetic energy part becomes more complicated and a regularization of the part is needed to avoid possible singularity, we gain the benefits that the optimization problem (1.7) is transformed to a convex one and the interaction energy terms are all in quadratic forms, the preferred form in a convex optimization problem. Via the finite difference method to discretize the regularized density function formulation and the accelerated projected gradient (APG) method to solve the optimization problem, we get the rDF-APG method. Comparison with the regularized Newton method shows that the method works for any $\beta \geq 0$ and $\delta \geq 0$, and is particularly suitable and efficient for the case with a strong HOI effect, i.e., $\delta \gg 1$.

The paper is organized as follows. In section 2, we introduce the regularized density function formulation for the problem (1.7) and prove rigorously the convergence of the corresponding ground state densities as the regularization effect vanishes. In section 3, we present the detailed finite difference discretization of the regularized den-

sity function formulation and analyze its spatial accuracy. In section 4, we adapt the APG method for solving the finite-dimensional discretized constraint minimization problem and describe the rDF-APG method in detail. Extensive numerical experiments are provided in section 5 to numerically verify the convergence and the spatial accuracy of the numerical ground state densities analyzed in the previous sections, and show the efficiency of the rDF-APG method when the interaction, especially the HOI effect, is strong. Finally, some conclusions are drawn in section 6.

2. A regularized density function formulation. In this section, we introduce the regularized density function formulation of the energy functional (1.4), and prove the convergence of the ground states as the regularization effect vanishes.

2.1. The formulation. When $\beta \geq 0$ and $\delta \geq 0$, it is sufficient to consider the positive wave function for the ground state [7]. Reformulating the energy functional (1.4) with the density function $\rho := |\phi|^2$, we get

$$E(\rho) = \int_{\mathbb{R}^d} \left[\frac{1}{2} |\nabla \sqrt{\rho}|^2 + V(\mathbf{x})\rho + \frac{\beta}{2}\rho^2 + \frac{\delta}{2} |\nabla \rho|^2 \right] d\mathbf{x}. \tag{2.1}$$

Then the ground state density $\rho_g = |\phi_g|^2$ can be defined as

$$\rho_g = \arg\min_{\rho \in W} E(\rho), \tag{2.2}$$

where

$$W := \left\{ \rho \;\middle|\; \int_{\mathbb{R}^d} \rho(\mathbf{x})\, d\mathbf{x} = 1,\ \rho \geq 0,\ E(\rho) < \infty \right\}. \tag{2.3}$$

Obviously, the feasible set of ρ in (2.2) is a simplex, which is convex, while the feasible set of ϕ in (1.4) is a nonconvex unit sphere. Combining with Lemma 2.1 below, we find that the optimization problem (2.2), which is formulated via the density function, is indeed a convex optimization problem if $\beta \geq 0$ and $\delta \geq 0$.

LEMMA 2.1. *When $\beta \geq 0$ and $\delta \geq 0$, $E(\rho)$ (2.1) is convex in W (2.3).*

Proof. The proof follows the same idea as shown in [6, 14] and is thus omitted for brevity. ∎

However, the algorithm based on direct minimization of the density formulated energy functional (2.1) suffers severely from the fact that $|\nabla \sqrt{\rho}|$ will go unbounded as $\rho \to 0^+$. On one hand, the unboundedness of $|\nabla \sqrt{\rho}|$ would introduce uncontrollable errors after discretization. On the other hand, the unboundedness of $|\nabla \sqrt{\rho}|$ implies the unboundedness of $\frac{\delta E}{\delta \rho}$, which will cause the slow convergence, or even the collapse, of most efficient optimization techniques. In fact, the above drawbacks will be numerically verified later in section 5. As a result, one expects that a regularization of the kinetic term is needed and the following regularized energy functional is considered:

$$\begin{aligned} E^\varepsilon(\rho) &= \int_{\mathbb{R}^d} \left[\frac{1}{2} |\nabla \sqrt{\rho + \varepsilon}|^2 + V(\mathbf{x})\rho + \frac{\beta}{2}\rho^2 + \frac{\delta}{2} |\nabla \rho|^2 \right] d\mathbf{x} \\ &= \int_{\mathbb{R}^d} \left[\frac{|\nabla \rho|^2}{8(\rho + \varepsilon)} + V(\mathbf{x})\rho + \frac{\beta}{2}\rho^2 + \frac{\delta}{2} |\nabla \rho|^2 \right] d\mathbf{x}, \quad \rho \in W, \end{aligned} \tag{2.4}$$

where $0 < \varepsilon \ll 1$ is a small regularization parameter. The convexity of $E^\varepsilon(\cdot)$ can be proved in a similar way and then we get Lemma 2.2.

LEMMA 2.2. *When $\beta \geq 0$ and $\delta \geq 0$, $E^\varepsilon(\rho)$ (2.4) is convex in W (2.3).*

The ground state density of the regularized energy functional $E^\varepsilon(\rho)$ (2.4) is defined as

$$\rho_g^\varepsilon = \arg\min_{\rho \in W} E^\varepsilon(\rho). \tag{2.5}$$

Later in this section, we show the convergence of the corresponding ground state densities as the regularization effect vanishes, i.e., $\lim_{\varepsilon \to 0^+} \rho_g^\varepsilon = \rho_g$, and characterize the convergence rate.

2.2. Existence and uniqueness. Before we study the convergence of ρ_g^ε (2.5), it is necessary to show the existence and uniqueness of the ground state density ρ_g^ε when $\beta \geq 0$ and $\delta \geq 0$. For simplicity, we introduce the function space

$$X_V = \left\{ \rho \,\middle|\, \|\rho\|_2 + \|\nabla \rho\|_2 + \int_{\mathbb{R}^d} V(\mathbf{x}) \rho \, d\mathbf{x} < \infty,\ \|\rho\|_1 = 1,\ \rho \geq 0 \right\}, \tag{2.6}$$

where $\|\rho\|_1 := \int_{\mathbb{R}^d} |\rho| \, d\mathbf{x}$ and $V(\mathbf{x})$ satisfies the confining condition, i.e.,

$$\lim_{|\mathbf{x}| \to \infty} V(\mathbf{x}) = +\infty. \tag{2.7}$$

We start with the following lemma.

LEMMA 2.3. *Suppose the external potential $V(\mathbf{x})$ satisfies the confining condition (2.7), then for any sequence $\{\rho_n\} \subset X_V$ such that $\int_{\mathbb{R}^d} V(\mathbf{x}) \rho_n \leq C$ for some constant C uniformly and $\rho_n \rightharpoonup \rho$ in $H^1(\mathbb{R}^d)$, we have $\rho \geq 0$, $\|\rho\|_1 = 1$, and $\rho_n \to \rho$ in $L^1(\mathbb{R}^d)$.*

Proof. For any $\eta > 0$, the confining condition of $V(\mathbf{x})$ (2.7) indicates that we can choose R large enough such that $V(\mathbf{x}) \geq \frac{4C}{\eta}$ for all $\mathbf{x} \in \Omega_R^c := \mathbb{R}^d \backslash \Omega_R$, where $\Omega_R = \{\mathbf{x} \,|\, |\mathbf{x}| < R\}$. Then $\int_{\Omega_R^c} \rho_n \, d\mathbf{x}$ is uniformly bounded by $\frac{\eta}{4}$ since

$$\int_{\Omega_R^c} \rho_n \, d\mathbf{x} \leq \frac{\eta}{4C} \int_{\Omega_R^c} V(\mathbf{x}) \rho_n \, d\mathbf{x} \leq \frac{\eta}{4C} \int_{\mathbb{R}^d} V(\mathbf{x}) \rho_n \, d\mathbf{x} \leq \frac{\eta}{4}. \tag{2.8}$$

In the bounded domain Ω_R, the weak convergence in H^1-norm implies $\rho_n \to \rho$ in the L^2-norm due to the Sobolev embedding theorem and, further, $\rho_n \to \rho$ in $L^1(\Omega_R)$ by the Hölder's inequality. Therefore, for all n large enough, we have

$$\int_{\Omega_R} |\rho_n - \rho| \, d\mathbf{x} \leq \frac{\eta}{2}. \tag{2.9}$$

Besides, we can choose a subsequence of $\{\rho_n\}$, denoted as the sequence itself for simplicity, which converges pointwisely to ρ in Ω_R. By Fatou's lemma,

$$\int_{\Omega_R} \rho \, d\mathbf{x} \leq \liminf_{n \to \infty} \int_{\Omega_R} \rho_n \, d\mathbf{x} \leq C. \tag{2.10}$$

Noticing that (2.10) can be extended to any bounded domain, we get $\int_{\mathbb{R}^d} \rho \, d\mathbf{x} \leq C$. Following an argument similar to (2.8), we have

$$\int_{\Omega_R^c} \rho \, d\mathbf{x} \leq \frac{\eta}{4}. \tag{2.11}$$

Combining (2.8), (2.9), and (2.11), we have that, for any given $\eta > 0$, $\int_{\mathbb{R}^d} |\rho - \rho_n| \, d\mathbf{x} \leq \eta$ if n is large enough, which indicates $\rho_n \to \rho$ in $L^1(\mathbb{R}^d)$ and $\|\rho\|_1 = 1$. The conclusion $\rho \geq 0$ comes from the pointwise convergence of a subsequence of $\{\rho_n\}$. The details are omitted here for brevity. ∎

With Lemma 2.3, we are ready to show the existence and uniqueness of the ground state density of the regularized energy functional. When $\delta = 0$ and $\beta \geq 0$, the existence and uniqueness of the ground state density is obvious. Here we focus on the case with $\delta > 0$ and an arbitrary $\beta \in \mathbb{R}$, and get the following theorem.

THEOREM 2.4 (existence and uniqueness). *Assume that $\delta > 0$ and $V(\mathbf{x}) \geq 0$ satisfies the confining condition* (2.7)*, then there exists a ground state density ρ_g^ε of the regularized energy functional $E^\varepsilon(\cdot)$* (2.4) *in W* (2.3)*. And the ground state density is unique if we further assume $\beta \geq 0$.*

Proof. To show the existence, we start with the following inequality,

$$\int_{\mathbb{R}^d} |\rho|^2 \, d\mathbf{x} \leq \left(\tilde{C} \int_{\mathbb{R}^d} \rho(\mathbf{x}) \, d\mathbf{x} \right)^{4/d+2} \|\nabla \rho\|_2^{2d/d+2} \leq \frac{\tilde{C}}{\eta} + \eta \|\nabla \rho\|_2^2 \tag{2.12}$$

for any $\eta > 0$, where the first inequality is due to the Nash inequality and the second one is due to Young's inequality. When $\beta \geq 0$, it is easy to see that $E^\varepsilon(\rho)$ is bounded from below. When $\beta < 0$, by choosing η such that $\eta|\beta| = \frac{\delta}{2}$, the inequality (2.12) immediately indicates that $E^\varepsilon(\rho)$ is bounded from below since

$$E^\varepsilon(\rho) \geq \int_{\mathbb{R}^d} \left(\frac{1}{2} |\nabla \sqrt{\rho + \varepsilon}|^2 + V(\mathbf{x})\rho + \frac{\delta}{4} |\nabla \rho|^2 \right) d\mathbf{x} - \frac{\tilde{C}\beta^2}{\delta}. \tag{2.13}$$

Taking a minimizing sequence $\{\rho_n\}$ in W, then $\{\rho_n\}$ is uniformly bounded in X_V with a weak limit ρ_∞ in the H^1-norm. Following a similar procedure to that shown in [7] and applying Lemma 2.3, we can show that ρ_∞ is indeed the ground state density. The details are omitted here for brevity.

If we further assume that $\beta \geq 0$, the uniqueness of the ground state density comes from the convexity of the regularized energy functional $E^\varepsilon(\rho)$ in ρ. ∎

2.3. Convergence of the ground states. In this section, we show the convergence of ρ_g^ε as $\varepsilon \to 0^+$, where ρ_g^ε is the ground state density of $E^\varepsilon(\cdot)$ (2.4). To begin with, we show the monotonicity of $E^\varepsilon(\cdot)$ as $\varepsilon \to 0^+$, which is simple but important in the proof of the convergence.

LEMMA 2.5. *For any fixed state $\rho \in X_V$*(2.6) *and $\varepsilon_1 \geq \varepsilon_2 \geq 0$, we have*

$$E^{\varepsilon_1}(\rho) \leq E^{\varepsilon_2}(\rho). \tag{2.14}$$

Proof. Noticing that $|\nabla \sqrt{\rho + \varepsilon_1}|^2 \leq |\nabla \sqrt{\rho + \varepsilon_2}|^2$ holds true for any $\rho \geq 0$ and $\varepsilon_1 \geq \varepsilon_2 \geq 0$, it is obvious that

$$E^{\varepsilon_1}(\rho) \leq E^{\varepsilon_2}(\rho). \tag{2.15}$$

∎

In particular, when $\beta \geq 0$ and $\delta \geq 0$, taking $\varepsilon_2 = 0$ and $\rho = \rho_g$ (2.2) in (2.15) and recalling the definition of ρ_g^ε (2.5), we have that

$$E^\varepsilon(\rho_g^\varepsilon) \leq E^\varepsilon(\rho_g) \leq E(\rho_g) \text{ for any } \varepsilon \geq 0. \tag{2.16}$$

With Lemma 2.5, we are ready to show the convergence of ρ_g^ε as $\varepsilon \to 0^+$. The result is summarized as the following theorem.

THEOREM 2.6. *For ground state densities ρ_g and ρ_g^ε defined in* (2.2) *and* (2.5) *with $\beta > 0$ and $\delta > 0$, respectively, we have $\rho_g^\varepsilon \to \rho_g$ in $H^1(\mathbb{R}^d)$ and*

$$\lim_{\varepsilon \to 0^+} E^\varepsilon(\rho_g^\varepsilon) = E(\rho_g). \tag{2.17}$$

Proof. The conclusion comes directly from the Γ-convergence of $E^\varepsilon(\cdot)$ as $\varepsilon \to 0^+$. In fact, it is sufficient to show the lower semicontinuity of $E^\varepsilon(\cdot)$ for all $\varepsilon \geq 0$ in X_V (2.6) with respect to the norm

$$\|\rho\|_V := \int_{\mathbb{R}^d} V(\mathbf{x})|\rho|\, d\mathbf{x} + \|\rho\|_{H^1} \tag{2.18}$$

since Lemma 2.5 indicates that the energy functional $E^\varepsilon(\cdot)$ is monotonically increasing as $\varepsilon \to 0^+$ [16]. Here we prove the lower semicontinuity of $E^\varepsilon(\cdot)$ via definition. To be more specific, for any convergent sequence $\{\rho_n\} \subset X_V$ (2.6) satisfying

$$\lim_{n\to\infty} \|\rho_n - \rho\|_V = 0 \tag{2.19}$$

for some $\rho \in X_V$, we aim to show that

$$\liminf_{n\to\infty} E^\varepsilon(\rho_n) \geq E^\varepsilon(\rho). \tag{2.20}$$

To begin with, we claim that

$$\nabla\sqrt{\rho_n + \varepsilon} \rightharpoonup \nabla\sqrt{\rho + \varepsilon} \quad \text{ in } L^2(\mathbb{R}^d). \tag{2.21}$$

Recalling the definition of the weak limit, we only need to show that

$$\lim_{n\to\infty} \int_{\mathbb{R}^d} \nabla\sqrt{\rho_n + \varepsilon}\, \phi\, d\mathbf{x} = \int_{\mathbb{R}^d} \nabla\sqrt{\rho + \varepsilon}\, \phi\, d\mathbf{x} \tag{2.22}$$

for any compactly supported smooth function ϕ. Here we assume $\mathrm{supp}(\phi) \subset \Omega_{\mathrm{R}} := \{\mathbf{x}\,|\,|\mathbf{x}| < \mathrm{R}\}$ for some $R > 0$. Obviously, $\rho_n \to \rho$ in $L^1(\Omega_R)$ by combining (2.19) and the Hölder inequality. A direct computation shows that

$$\limsup_{n\to\infty} \int_{\Omega_R} \left|\sqrt{\rho_n + \varepsilon} - \sqrt{\rho + \varepsilon}\right| d\mathbf{x} \leq \limsup_{n\to\infty} \int_{\Omega_R} \frac{|\rho_n - \rho|}{2\sqrt{\varepsilon}}\, d\mathbf{x} = 0, \tag{2.23}$$

which implies (2.22) and, thus, (2.21), immediately by combining the fact that

$$\int_{\mathbb{R}^d} \left(\nabla\sqrt{\rho_n + \varepsilon} - \nabla\sqrt{\rho + \varepsilon}\right) \phi\, d\mathbf{x} = -\int_{\Omega_R} \left(\sqrt{\rho_n + \varepsilon} - \sqrt{\rho + \varepsilon}\right) \nabla\phi\, d\mathbf{x}, \tag{2.24}$$

and the fact that ϕ is smooth and compactly supported within Ω_R.

By the weak convergence (2.21), we have that

$$\liminf_{n\to\infty} \|\nabla\sqrt{\rho_n + \varepsilon}\|_2 \geq \|\nabla\sqrt{\rho + \varepsilon}\|_2. \tag{2.25}$$

On the other hand, the convergence of $\{\rho_n\}$ in the sense (2.19) implies that

$$\lim_{n\to\infty} \int_{\mathbb{R}^d} V(\mathbf{x})\rho_n\, d\mathbf{x} = \int_{\mathbb{R}^d} V(\mathbf{x})\rho\, d\mathbf{x} \tag{2.26}$$

and

$$\lim_{n\to\infty} \|\rho_n\|_2 = \|\rho\|_2, \quad \lim_{n\to\infty} \|\nabla\rho_n\|_2 = \|\nabla\rho\|_2. \tag{2.27}$$

Thus we proved the lower semicontinuity of $E^\varepsilon(\cdot)$ (2.20). ∎

Remark 2.7. One key step (2.23) in the proof is no longer valid when $\varepsilon = 0$. However, we can still prove the lower semicontinuity of the energy functional $E^0(\cdot)$ via a similar, but more complicated, argument.

Theorem 2.6 shows the convergence of ρ_g^ε. Although the exact convergence rate is unclear, the theorem below shows a relation between the convergence rate of the ground state density ρ_g^ε (2.5) and the convergence rate of the corresponding energy.

THEOREM 2.8. *For ρ_g and ρ_g^ε defined in* (2.2) *and* (2.5) *with $\beta \geq 0$ and $\delta \geq 0$, respectively, we have*

$$\frac{\beta}{2}\|\rho_g - \rho_g^\varepsilon\|_2^2 + \frac{\delta}{2}\|\nabla(\rho_g - \rho_g^\varepsilon)\|_2^2 \leq E(\rho_g) - E^\varepsilon(\rho_g^\varepsilon). \tag{2.28}$$

Proof. We start by proving the following lemma, which plays an essential role in the proof of (2.28).

LEMMA 2.9. *Define $R(\rho_g, \rho_g^\varepsilon) = \int_{\mathbb{R}^d} \left(\beta\rho_g^\varepsilon - \delta\Delta\rho_g^\varepsilon\right)(\rho_g - \rho_g^\varepsilon)\, d\mathbf{x}$ and $I(\rho_g, \rho_g^\varepsilon) = \int_{\mathbb{R}^d} V(\mathbf{x})(\rho_g - \rho_g^\varepsilon)\, d\mathbf{x}$, then*

$$R(\rho_g, \rho_g^\varepsilon) + I(\rho_g, \rho_g^\varepsilon) \geq \int_{\mathbb{R}^d} \left[-\frac{\nabla\rho_g^\varepsilon \cdot \nabla(\rho_g - \rho_g^\varepsilon)}{4(\rho_g^\varepsilon + \varepsilon)} + \frac{|\nabla\rho_g^\varepsilon|^2(\rho_g - \rho_g^\varepsilon)}{8(\rho_g^\varepsilon + \varepsilon)^2} \right] d\mathbf{x}. \tag{2.29}$$

To prove Lemma 2.9, we consider $f(t) = E^\varepsilon(\rho_g^\varepsilon + t(\rho_g - \rho_g^\varepsilon))$. Obviously, $\rho_g^\varepsilon + t(\rho_g - \rho_g^\varepsilon) \in W$ (2.3) for any $t \in [0, 1]$. Therefore, $f(t)$ takes its minimum value in $[0, 1]$ at $t = 0$ by recalling the definition of ρ_g^ε (2.5), which indicates $f'(0) \geq 0$. A direct computation of $f'(0)$ shows that the requirement $f'(0) \geq 0$ is exactly (2.29). The details are omitted here for brevity.

Now we come back to the proof of (2.28). For simplicity, we define

$$K(\rho_g, \rho_g^\varepsilon) = \int_{\mathbb{R}^d} \left[\frac{1}{2}|\nabla\sqrt{\rho_g}|^2 - \frac{1}{2}|\nabla\sqrt{\rho_g^\varepsilon + \varepsilon}|^2 \right] d\mathbf{x} \tag{2.30}$$

and

$$D(\rho_g, \rho_g^\varepsilon) = \frac{\beta}{2}\|\rho_g - \rho_g^\varepsilon\|_2^2 + \frac{\delta}{2}\|\nabla(\rho_g - \rho_g^\varepsilon)\|_2^2. \tag{2.31}$$

Then, by a direct computation, we have that

$$\int_{\mathbb{R}^d} \left[\frac{\beta}{2}(|\rho_g|^2 - |\rho_g^\varepsilon|^2) + \frac{\delta}{2}(|\nabla\rho_g|^2 - |\nabla\rho_g^\varepsilon|^2) \right] d\mathbf{x} = R(\rho_g, \rho_g^\varepsilon) + D(\rho_g, \rho_g^\varepsilon) \tag{2.32}$$

and, therefore,

$$\begin{aligned}
E(\rho_g) - E^\varepsilon(\rho_g^\varepsilon) &= K(\rho_g, \rho_g^\varepsilon) + I(\rho_g, \rho_g^\varepsilon) + R(\rho_g, \rho_g^\varepsilon) + D(\rho_g, \rho_g^\varepsilon) \\
&\geq K(\rho_g, \rho_g^\varepsilon) \\
&\quad + \int_{\mathbb{R}^d} \left[-\frac{\nabla\rho_g^\varepsilon \cdot \nabla(\rho_g - \rho_g^\varepsilon)}{4(\rho_g^\varepsilon + \varepsilon)} + \frac{|\nabla\rho_g^\varepsilon|^2(\rho_g - \rho_g^\varepsilon)}{8(\rho_g^\varepsilon + \varepsilon)^2} \right] d\mathbf{x} + D(\rho_g, \rho_g^\varepsilon) \\
&= \int_{\mathbb{R}^d} \left[\frac{|\nabla\rho_g|^2}{8\rho_g} + \frac{|\nabla\rho_g^\varepsilon|^2(\rho_g + \varepsilon)}{8(\rho_g^\varepsilon + \varepsilon)^2} - \frac{\nabla\rho_g^\varepsilon \cdot \nabla\rho_g}{4(\rho_g^\varepsilon + \varepsilon)} \right] d\mathbf{x} + D(\rho_g, \rho_g^\varepsilon) \\
&\geq \int_{\mathbb{R}^d} \left[\frac{|\nabla\rho_g||\nabla\rho_g^\varepsilon|}{4(\rho_g^\varepsilon + \varepsilon)} - \frac{\nabla\rho_g^\varepsilon \cdot \nabla\rho_g}{4(\rho_g^\varepsilon + \varepsilon)} \right] d\mathbf{x} + D(\rho_g, \rho_g^\varepsilon) \geq D(\rho_g, \rho_g^\varepsilon),
\end{aligned} \tag{2.33}$$

where the first inequality is due to Lemma 2.9, the last two inequalities are by Young's inequality and the Cauchy–Schwarz inequality, respectively. ∎

Remark 2.10. The error estimate in Theorem 2.8 is suboptimal. Later, in section 5, we will show that, in some specific setting, we observe the asymptotic error of order $O(\varepsilon)$ in both energy and the L^2-norm. However, only the $O(\sqrt{\varepsilon})$ error in the L^2-norm can be expected via Theorem 2.8.

3. Numerical discretization. In this section, we present the detailed spatial discretization of the regularized energy functional $E^\varepsilon(\cdot)$ (2.4). The second order finite difference method is applied to discretize the energy functional in the regularized density function formulation and the spatial accuracy of the corresponding numerical ground state density is analyzed in details.

3.1. A second order finite difference discretization. Due to the exponential decay of the ground state under the confining external potential (2.7) [7], it is reasonable to truncate the problem on a bounded, but sufficiently large domain with the homogeneous Dirichlet boundary condition imposed. For simplicity, only the case in one dimension (1D) is considered here. Extensions to higher dimensions for tensor grids are straightforward.

In 1D, truncate the problem into an interval $U = (a, b)$ and choose the uniform grid points as

$$x_j = a + jh \text{ for } j = 0, 1, \ldots, N \tag{3.1}$$

with mesh size $h = (b - a)/N$. Let ρ_j be the numerical approximation of $\rho(x_j)$ and denote $\boldsymbol{\rho}_h$ to be the vector of length $N - 1$ with its jth component to be ρ_j, i.e.,

$$\boldsymbol{\rho}_h = (\rho_1, \ldots, \rho_{N-1})^T \in \mathbb{R}^{N-1}. \tag{3.2}$$

By the homogenous Dirichlet boundary condition, we have $\rho_0 = \rho_N = 0$. Define the discrete norms of the vector $\boldsymbol{\rho}_h$ as

$$\|\boldsymbol{\rho}_h\|_{l^1} := h \sum_{j=1}^{N-1} |\rho_j|, \ \|\boldsymbol{\rho}_h\|_{l^2} := \sqrt{h \sum_{j=1}^{N-1} |\rho_j|^2}, \ \|\delta_x^+ \boldsymbol{\rho}_h\|_{l^2} := \sqrt{h \sum_{j=0}^{N-1} |\delta_x^+ \rho_j|^2}, \tag{3.3}$$

where δ_x^+, which is the finite difference approximation of ∂_x, is defined as $\delta_x^+ \rho_j := (\rho_{j+1} - \rho_j)/h$. Then the feasible set W_h can be defined as

$$W_h = \{\boldsymbol{\rho}_h = (\rho_1, \ldots, \rho_{N-1})^T \in \mathbb{R}^{N-1} \,|\, \|\boldsymbol{\rho}_h\|_{l^1} = 1, \boldsymbol{\rho}_h \geq 0\}. \tag{3.4}$$

With the notations defined above, we are now ready to discretize the regularized energy functional $E^\varepsilon(\cdot)$ (2.4) in 1D. Noticing the boundary condition $\rho_0 = \rho_N = 0$, we have

$$\begin{aligned}
E^\varepsilon(\rho) &= \int_a^b \left[\frac{|\partial_x \rho|^2}{8(\rho + \varepsilon)} + V(x)\rho + \frac{\beta}{2}\rho^2 + \frac{\delta}{2}|\partial_x \rho|^2 \right] dx \\
&= \int_a^b \left[\frac{|\partial_x \rho|^2}{8(\rho + \varepsilon)} + \frac{\delta}{2}|\partial_x \rho|^2 \right] dx + \int_a^b \left[V(x)\rho + \frac{\beta}{2}\rho^2 \right] dx \\
&\approx h \sum_{j=0}^{N-1} \left[\frac{1}{8} \frac{|\delta_x^+ \rho_j|^2}{\rho_{j+\frac{1}{2}} + \varepsilon} + \frac{\delta}{2} \left|\delta_x^+ \rho_j\right|^2 \right] + h \sum_{j=0}^{N-1} \left[V(x_j)\rho_j + \frac{\beta}{2}\rho_j^2 \right] \\
&\approx h \sum_{j=0}^{N-1} \left[\frac{1}{4} \frac{|\delta_x^+ \rho_j|^2}{\rho_j + \rho_{j+1} + 2\varepsilon} + V(x_j)\rho_j + \frac{\beta}{2}\rho_j^2 + \frac{\delta}{2} \left|\delta_x^+ \rho_j\right|^2 \right],
\end{aligned} \tag{3.5}$$

where we approximate the first integral on the second line via the composite midpoint rule and the second integral via the composite trapezoidal rule. Define

$$E_h^\varepsilon(\boldsymbol{\rho}_h) = h\sum_{j=0}^{N-1}\left[\frac{1}{4}\frac{|\delta_x^+\rho_j|^2}{\rho_j+\rho_{j+1}+2\varepsilon} + V(x_j)\rho_j + \frac{\beta}{2}\rho_j^2 + \frac{\delta}{2}\left|\delta_x^+\rho_j\right|^2\right], \tag{3.6}$$

where $\boldsymbol{\rho}_h \in W_h$ (3.4) and $\rho_0 = \rho_N = 0$. The problem (2.5) now becomes finding $\boldsymbol{\rho}_{g,h}^\varepsilon = (\rho_{g,1}^\varepsilon, \rho_{g,2}^\varepsilon, \ldots, \rho_{g,N-1}^\varepsilon)^T \in W_h$ such that

$$\boldsymbol{\rho}_{g,h}^\varepsilon = \operatorname*{arg\,min}_{\boldsymbol{\rho}_h\in W_h} E_h^\varepsilon(\boldsymbol{\rho}_h). \tag{3.7}$$

And the corresponding numerical energy $E_{g,h}^\varepsilon := E_h^\varepsilon(\boldsymbol{\rho}_{g,h}^\varepsilon)$ approximates $E^\varepsilon(\rho_g^\varepsilon)$.

By Theorem 2.6, the ground state density ρ_g^ε of the regularized energy functional (2.4) will converge to the ground state density ρ_g of (2.1) as $\varepsilon \to 0^+$. Therefore, to solve the original optimization problem (2.2), we only need to choose a sufficiently small ε and find the corresponding numerical ground state density $\boldsymbol{\rho}_{g,h}^\varepsilon$ as an approximation.

We claim that the problem (3.7) is a finite-dimensional convex optimization problem. The convexity of the feasible set W_h (3.4) is obvious. And the convexity of $E_h^\varepsilon(\cdot)$ is shown in Lemma 3.1 below.

LEMMA 3.1. *If $\beta \ge 0$ and $\delta \ge 0$, the discretized energy functional $E_h^\varepsilon(\cdot)$ (3.6) is convex in the feasible set W_h (3.4) for any fixed $\varepsilon \ge 0$.*

Proof. The convexity of the external potential term and the last two quadratic terms in (3.6) is obvious. Therefore, we only need to show the convexity of the kinetic energy term, i.e., the first term, in (3.6). Define $E^{\mathrm{kin}}(\boldsymbol{\rho}_h) = \sum_{j=0}^{N-1} E_j^{\mathrm{kin}}(\boldsymbol{\rho}_h)$, where

$$E_j^{\mathrm{kin}}(\boldsymbol{\rho}_h) := \frac{1}{4h^2}\frac{|\rho_{j+1}-\rho_j|^2}{\rho_j+\rho_{j+1}+2\varepsilon}. \tag{3.8}$$

For any two vectors $\mathbf{a}_h = (a_1, \ldots, a_{N-1})^T \in W_h$ and $\mathbf{b}_h = (b_1, \ldots, b_{N-1})^T \in W_h$ with $a_0 = a_N = b_0 = b_N = 0$, a direct computation shows that, for any $j = 0, 1, \ldots, N-1$,

$$\begin{aligned}
\frac{E_j^{\mathrm{kin}}(\mathbf{a}_h) + E_j^{\mathrm{kin}}(\mathbf{b}_h)}{2} &= \frac{1}{8h^2}\left(\frac{|a_{j+1}-a_j|^2}{a_j+a_{j+1}+2\varepsilon} + \frac{|b_{j+1}-b_j|^2}{b_j+b_{j+1}+2\varepsilon}\right)\\
&= \frac{1}{8h^2}\frac{|a_{j+1}-a_j|^2\left(1+\frac{b_j+b_{j+1}+2\varepsilon}{a_j+a_{j+1}+2\varepsilon}\right) + |b_{j+1}-b_j|^2\left(1+\frac{a_j+a_{j+1}+2\varepsilon}{b_j+b_{j+1}+2\varepsilon}\right)}{(a_j+a_{j+1}+2\varepsilon)+(b_j+b_{j+1}+2\varepsilon)}\\
&\ge \frac{1}{8h^2}\frac{(a_{j+1}-a_j)^2+(b_{j+1}-b_j)^2+2(a_{j+1}-a_j)(b_{j+1}-b_j)}{(a_j+a_{j+1}+2\varepsilon)+(b_j+b_{j+1}+2\varepsilon)}\\
&= \frac{1}{8h^2}\frac{|a_{j+1}+b_{j+1}-a_j-b_j|^2}{(a_j+a_{j+1}+2\varepsilon)+(b_j+b_{j+1}+2\varepsilon)} = E_j^{\mathrm{kin}}\left(\frac{\mathbf{a}_h+\mathbf{b}_h}{2}\right),
\end{aligned} \tag{3.9}$$

where the inequality is due to the Cauchy inequality, which shows the convexity of $E_j^{\mathrm{kin}}(\cdot)$. The convexity of $E^{\mathrm{kin}}(\cdot)$ is then obvious. ∎

The existence and uniqueness of the ground state density $\boldsymbol{\rho}_{g,h}^\varepsilon$ (3.7) for a fixed $\varepsilon \ge 0$ when $\beta \ge 0$ and $\delta \ge 0$ come directly from the fact that the convex function $E_h^\varepsilon(\cdot)$ is bounded below by 0.

To solve the problem (3.7), it is usually important to get the gradient of the discretized energy functional $E_h^\varepsilon(\boldsymbol{\rho}_h)$ since most efficient optimization techniques are gradient-based. Denote

$$\mathbf{g}_h^\varepsilon(\boldsymbol{\rho}_h) = \left(\frac{\partial E_h^\varepsilon}{\partial \rho_1}, \frac{\partial E_h^\varepsilon}{\partial \rho_2}, \ldots, \frac{\partial E_h^\varepsilon}{\partial \rho_{N-1}}\right)^T. \tag{3.10}$$

Then its jth component can be explicitly computed as

$$\mathbf{g}_h^\varepsilon[j] := \frac{\partial E_h^\varepsilon}{\partial \rho_j} = h\left[-\frac{\delta_x^+ f_{j-1}}{2} - \frac{f_{j-1}^2 + f_j^2}{4} + V(x_j) + \beta\rho_j - \delta(\delta_x^2\rho_j)\right], \tag{3.11}$$

where $\delta_x^2\rho_j := (\rho_{j+1} - 2\rho_j + \rho_{j-1})/h^2$ for $j = 1, 2, \ldots, N-1$ and

$$f_j = f_j(\boldsymbol{\rho}_h) := \frac{\delta_x^+\rho_j}{\rho_j + \rho_{j+1} + 2\varepsilon} \quad \text{for } j = 0, 1, \ldots, N-1. \tag{3.12}$$

The energy functional $E_h^\varepsilon(\boldsymbol{\rho}_h)$ (3.6) and its gradient $\mathbf{g}_h^\varepsilon(\boldsymbol{\rho}_h)$ (3.11) can be written in a more concise form. Define a symmetric matrix $A = (a_{jk}) \in \mathbb{R}^{(N-1)\times(N-1)}$, where

$$a_{jk} = \frac{1}{h^2}\begin{cases} 2 & \text{if } j = k, \\ -1 & \text{if } j = k \pm 1, \\ 0 & \text{otherwise.} \end{cases} \tag{3.13}$$

Then we have $E_h^\varepsilon(\boldsymbol{\rho}_h)$ (3.6) and $\mathbf{g}_h^\varepsilon(\boldsymbol{\rho}_h)$ (3.11) in compact forms as

$$E_h^\varepsilon(\boldsymbol{\rho}_h) = hE^{\mathrm{kin}}(\boldsymbol{\rho}_h) + h\left[\mathbf{v}^T\boldsymbol{\rho}_h + \frac{\beta}{2}\boldsymbol{\rho}_h^T\boldsymbol{\rho}_h + \delta\boldsymbol{\rho}_h^T A\boldsymbol{\rho}_h\right], \tag{3.14}$$

$$\mathbf{g}_h^\varepsilon(\boldsymbol{\rho}_h) = h\nabla E^{\mathrm{kin}}(\boldsymbol{\rho}_h) + h\left[\mathbf{v} + \beta\boldsymbol{\rho}_h + 2\delta A\boldsymbol{\rho}_h\right], \tag{3.15}$$

respectively, where $E^{\mathrm{kin}}(\boldsymbol{\rho}_h) = \sum_{j=0}^{N-1} E_j^{\mathrm{kin}}(\boldsymbol{\rho}_h)$ with $E_j^{\mathrm{kin}}(\boldsymbol{\rho}_h)$ defined in (3.8), $\mathbf{v} = (V(x_1), V(x_2), \ldots, V(x_{N-1}))^T \in \mathbb{R}^{N-1}$, and

$$\nabla E^{\mathrm{kin}}(\boldsymbol{\rho}_h) = \left(\frac{\partial E^{\mathrm{kin}}(\boldsymbol{\rho}_h)}{\partial \rho_1}, \frac{\partial E^{\mathrm{kin}}(\boldsymbol{\rho}_h)}{\partial \rho_2}, \ldots, \frac{\partial E^{\mathrm{kin}}(\boldsymbol{\rho}_h)}{\partial \rho_{N-1}}\right)^T \in \mathbb{R}^{N-1} \tag{3.16}$$

with

$$\frac{\partial E^{\mathrm{kin}}(\boldsymbol{\rho}_h)}{\partial \rho_j} = -\frac{\delta_x^+ f_{j-1}}{2} - \frac{f_{j-1}^2 + f_j^2}{4}, \tag{3.17}$$

where $f_j = f_j(\boldsymbol{\rho}_h)$ is defined in (3.12).

3.2. Spatial error analysis. In this section, we study the spatial accuracy of the numerical ground state density. For simplicity, only the 1-dimensional case is considered here. The following theorem can be proved, which shows that the difference between the ground state density $\boldsymbol{\rho}_{g,h}^\varepsilon$ (3.7) and an arbitrary vector $\boldsymbol{\rho}_h \in W_h$ (3.4) is closely related to the difference of the corresponding energies.

THEOREM 3.2. *Considering the ground state density* $\boldsymbol{\rho}_{g,h}^\varepsilon = (\rho_{g,1}^\varepsilon, \rho_{g,2}^\varepsilon, \ldots, \rho_{g,N-1}^\varepsilon)^T$ (3.7) *and an arbitrary vector* $\boldsymbol{\rho}_h = (\rho_1, \rho_2, \ldots, \rho_{N-1})^T$ *in* W_h (3.4)*, we have*

$$\frac{\beta}{2}\|\boldsymbol{\rho}_h - \boldsymbol{\rho}_{g,h}^\varepsilon\|_{l^2}^2 + \frac{\delta}{2}\|\delta_x^+(\boldsymbol{\rho}_h - \boldsymbol{\rho}_{g,h}^\varepsilon)\|_{l^2}^2 \le E_h^\varepsilon(\boldsymbol{\rho}_h) - E_h^\varepsilon(\boldsymbol{\rho}_{g,h}^\varepsilon). \tag{3.18}$$

Proof. We follow a similar procedure as in the proof of Theorem 2.8. Define

$$f(t) = E_h^\varepsilon(\boldsymbol{\rho}_{g,h}^\varepsilon + t(\boldsymbol{\rho}_h - \boldsymbol{\rho}_{g,h}^\varepsilon)), \quad \text{where } t \in [0,1]. \tag{3.19}$$

Noticing that $\boldsymbol{\rho}_{g,h}^\varepsilon$ minimizes $E_h^\varepsilon(\cdot)$ in W_h (3.4), we have

$$f'(0) = (\mathbf{g}_h^\varepsilon(\boldsymbol{\rho}_{g,h}^\varepsilon))^T(\boldsymbol{\rho}_h - \boldsymbol{\rho}_{g,h}^\varepsilon) \geq 0, \tag{3.20}$$

where $\mathbf{g}_h^\varepsilon$ is defined in (3.15). Substituting (3.15) into (3.20), we get

$$\mathbf{v}^T(\boldsymbol{\rho}_h - \boldsymbol{\rho}_{g,h}^\varepsilon) + R(\boldsymbol{\rho}_h, \boldsymbol{\rho}_{g,h}^\varepsilon) \geq -\left[\nabla E^{\mathrm{kin}}(\boldsymbol{\rho}_{g,h}^\varepsilon)\right]^T(\boldsymbol{\rho}_h - \boldsymbol{\rho}_{g,h}^\varepsilon), \tag{3.21}$$

where

$$R(\boldsymbol{\rho}_h, \boldsymbol{\rho}_{g,h}^\varepsilon) = \left[\beta\boldsymbol{\rho}_{g,h}^\varepsilon + 2\delta A\boldsymbol{\rho}_{g,h}^\varepsilon\right]^T(\boldsymbol{\rho}_h - \boldsymbol{\rho}_{g,h}^\varepsilon). \tag{3.22}$$

On the other hand, a direct computation shows that

$$E_h^\varepsilon(\boldsymbol{\rho}_h) - E_h^\varepsilon(\boldsymbol{\rho}_{g,h}^\varepsilon) = h\left[E^{\mathrm{kin}}(\boldsymbol{\rho}_h) - E^{\mathrm{kin}}(\boldsymbol{\rho}_{g,h}^\varepsilon)\right] + h\mathbf{v}^T(\boldsymbol{\rho}_h - \boldsymbol{\rho}_{g,h}^\varepsilon) + I_1, \tag{3.23}$$

where the difference of the interaction energy is contained in the term I_1, which can be explicitly computed as

$$I_1 = \frac{h\beta}{2}\left[(\boldsymbol{\rho}_h)^T\boldsymbol{\rho}_h - (\boldsymbol{\rho}_{g,h}^\varepsilon)^T\boldsymbol{\rho}_{g,h}^\varepsilon\right] + h\delta\left[(\boldsymbol{\rho}_h)^TA\boldsymbol{\rho}_h - (\boldsymbol{\rho}_{g,h}^\varepsilon)^TA\boldsymbol{\rho}_{g,h}^\varepsilon\right]. \tag{3.24}$$

Noticing that $h\boldsymbol{\rho}_h^TA\boldsymbol{\rho}_h = \|\delta_x^+\boldsymbol{\rho}_h\|_{l^2}^2$ holds true for any $\boldsymbol{\rho}_h \in W_h$ and $A^T = A$, we have

$$\begin{aligned} I_1 &= h\left(\frac{\beta}{2}(\boldsymbol{\rho}_h + \boldsymbol{\rho}_{g,h}^\varepsilon) + \delta A(\boldsymbol{\rho}_h + \boldsymbol{\rho}_{g,h}^\varepsilon)\right)^T(\boldsymbol{\rho}_h - \boldsymbol{\rho}_{g,h}^\varepsilon) \\ &= hR(\boldsymbol{\rho}_h, \boldsymbol{\rho}_{g,h}^\varepsilon) + D(\boldsymbol{\rho}_h, \boldsymbol{\rho}_{g,h}^\varepsilon), \end{aligned} \tag{3.25}$$

where $D(\boldsymbol{\rho}_h, \boldsymbol{\rho}_{g,h}^\varepsilon) = \frac{\beta}{2}\|\boldsymbol{\rho}_h - \boldsymbol{\rho}_{g,h}^\varepsilon\|_{l^2}^2 + \frac{\delta}{2}\|\delta_x^+(\boldsymbol{\rho}_h - \boldsymbol{\rho}_{g,h}^\varepsilon)\|_{l^2}^2$ and, therefore,

$$\begin{aligned} E_h^\varepsilon(\boldsymbol{\rho}_h) - E_h^\varepsilon(\boldsymbol{\rho}_{g,h}^\varepsilon) &= h\left[E^{\mathrm{kin}}(\boldsymbol{\rho}_h) - E^{\mathrm{kin}}(\boldsymbol{\rho}_{g,h}^\varepsilon)\right] \\ &\quad + h[\mathbf{v}^T(\boldsymbol{\rho}_h - \boldsymbol{\rho}_{g,h}^\varepsilon) + R(\boldsymbol{\rho}_h, \boldsymbol{\rho}_{g,h}^\varepsilon)] + D(\boldsymbol{\rho}_h, \boldsymbol{\rho}_{g,h}^\varepsilon) \\ &\geq h\left[E^{\mathrm{kin}}(\boldsymbol{\rho}_h) - E^{\mathrm{kin}}(\boldsymbol{\rho}_{g,h}^\varepsilon)\right] \\ &\quad - h\left[\nabla E^{\mathrm{kin}}(\boldsymbol{\rho}_{g,h}^\varepsilon)\right]^T(\boldsymbol{\rho}_h - \boldsymbol{\rho}_{g,h}^\varepsilon) + D(\boldsymbol{\rho}_h, \boldsymbol{\rho}_{g,h}^\varepsilon) \\ &\geq D(\boldsymbol{\rho}_h, \boldsymbol{\rho}_{g,h}^\varepsilon), \end{aligned} \tag{3.26}$$

where the first inequality is due to (3.21) and the second inequality is due to the convexity of $E^{\mathrm{kin}}(\cdot)$ in W_h (3.4), which is proved in Lemma 3.1. The above inequality is exactly what we aim to show in Theorem 3.2 noticing the definition of $D(\boldsymbol{\rho}_h, \boldsymbol{\rho}_{g,h}^\varepsilon)$. ∎

Theorem 3.2 offers a way to measure the difference between a general state and the ground state by considering the difference of the corresponding energies when $\beta > 0$ and $\delta > 0$. In particular, we can study the discrete error estimates based on Theorem 3.2. For simplicity, we use the notation $\Pi_h\rho_g^\varepsilon$ to be the interpolation of the ground state ρ_g^ε (2.5) on the grid points, i.e.,

$$\Pi_h\rho_g^\varepsilon = (\rho_g^\varepsilon(x_1), \rho_g^\varepsilon(x_2), \ldots, \rho_g^\varepsilon(x_{N-1}))^T \in \mathbb{R}^{N-1}, \tag{3.27}$$

then we have the following result measuring the difference $\Pi_h\rho_g^\varepsilon - \boldsymbol{\rho}_{g,h}^\varepsilon$.

THEOREM 3.3. *Fix $\varepsilon > 0$ and consider $\mathbf{e}_h^\varepsilon = \Pi_h \rho_g^\varepsilon - \boldsymbol{\rho}_{g,h}^\varepsilon$. If $\beta > 0$ and $\delta > 0$, then we have*

$$\|\delta_+ \mathbf{e}_h^\varepsilon\|_{l^2} \lesssim h, \quad \|\mathbf{e}_h^\varepsilon\|_{l^2} \lesssim h. \tag{3.28}$$

Proof. Denote C_h to be the scaling constant such that $C_h \|\Pi_h \rho_g^\varepsilon\|_{l^1} = 1$. Then $C_h \Pi_h \rho_g^\varepsilon \in W_h$ (3.4). Noticing that $\|\Pi_h \rho_g^\varepsilon\|_{l^1}$ approximates $\|\rho_g^\varepsilon\|_1 = 1$ via the composite trapezoidal rule, we have that

$$\|\Pi_h \rho_g^\varepsilon\|_{l^1} - 1 = \|\Pi_h \rho_g^\varepsilon\|_{l^1} - \int_a^b \rho_g^\varepsilon \, dx = \frac{b-a}{12} \partial_x^2 \rho_g^\varepsilon(\xi) h^2 \tag{3.29}$$

for some $\xi \in (a, b)$. As a result,

$$|C_h - 1| \le C_1 h^2 \tag{3.30}$$

for some C_1 depending on $\|\partial_x^2 \rho_g^\varepsilon\|_\infty$, when h is sufficiently small.

Notice that $\frac{1}{4} \frac{|\delta_x^+ \rho_j|^2}{\rho_j + \rho_{j+1} + 2\varepsilon}$ and $\delta_x^+ \rho_j$ are the second order accurate approximations of $\frac{1}{2} |\partial_x \sqrt{\rho_g^\varepsilon + \varepsilon}|^2$ and $\partial_x \rho_g^\varepsilon$ at $x = x_{j+\frac{1}{2}}$, respectively. It is then obvious that $E_h^\varepsilon(\cdot)$ approximates $E^\varepsilon(\cdot)$ by combing two second order accurate quadratures, i.e., the composite midpoint rule and the composite trapezoidal rule. Following a similar procedure, we get

$$|E^\varepsilon(\rho_g^\varepsilon) - E_h^\varepsilon(C_h \Pi_h \rho_g^\varepsilon)| \le C_2 h^2, \tag{3.31}$$

where the constant C_2 depends on $\|\partial_x^l \rho_g^\varepsilon\|_\infty$ for $l = 0, 1, 2, 3$.

Besides, if we consider the positive piecewise linear function $\tilde{\rho}_g^\varepsilon(x)$ such that $\tilde{\rho}_g^\varepsilon(x_j) = \rho_{g,j}^\varepsilon$, then $\tilde{\rho}_g^\varepsilon \in W$ (2.3) and $\frac{\delta}{2} |\partial_x \tilde{\rho}_g^\varepsilon|^2$ is piecewise constant. A similar, but more careful analysis, shows that

$$E^\varepsilon(\tilde{\rho}_g^\varepsilon) \le E_h^\varepsilon(\boldsymbol{\rho}_{g,h}^\varepsilon) + C_3 h^2, \tag{3.32}$$

where the constant C_3 depends on the uniform bound of $\|\delta_x^+ \boldsymbol{\rho}_{g,h}^\varepsilon\|_{l^2}$ with respect to h. The bound can be expressed via $E^\varepsilon(\rho_g^\varepsilon)$. The details are omitted here for brevity.

Recalling Theorem 3.2, we have

$$\begin{aligned} &\frac{\beta}{2} \|C_h \Pi_h \rho_g^\varepsilon - \boldsymbol{\rho}_{g,h}^\varepsilon\|_{l^2}^2 + \frac{\delta}{2} \|\delta_+ (C_h \Pi_h \rho_g^\varepsilon - \boldsymbol{\rho}_{g,h}^\varepsilon)\|_{l^2}^2 \le E_h^\varepsilon(C_h \Pi_h \rho_g^\varepsilon) - E_h^\varepsilon(\boldsymbol{\rho}_{g,h}^\varepsilon) \\ &\le E^\varepsilon(\rho_g^\varepsilon) - E^\varepsilon(\tilde{\rho}_g^\varepsilon) + (C_2 + C_3) h^2 \le (C_2 + C_3) h^2. \end{aligned} \tag{3.33}$$

The fact that $E^\varepsilon(\rho_g^\varepsilon) \le E^\varepsilon(\tilde{\rho}_g^\varepsilon)$ is applied in the last step. For $\beta > 0$ and $\delta > 0$, it is then obvious that

$$\|C_h \Pi_h \rho_g^\varepsilon - \boldsymbol{\rho}_{g,h}^\varepsilon\|_{l^2} \lesssim h \text{ and } \|\delta_+ (C_h \Pi_h \rho_g^\varepsilon - \boldsymbol{\rho}_{g,h}^\varepsilon)\|_{l^2} \lesssim h, \tag{3.34}$$

which further implies that

$$\|\mathbf{e}_h^\varepsilon\|_{l^2} \le \|C_h \Pi_h \rho_g^\varepsilon - \boldsymbol{\rho}_{g,h}^\varepsilon\|_{l^2} + |C_h - 1| \|\Pi_h \rho_g^\varepsilon\|_{l^2} \lesssim h \tag{3.35}$$

and

$$\|\delta_+ \mathbf{e}_h^\varepsilon\|_{l^2} \le \|\delta_+ (C_h \Pi_h \rho_g^\varepsilon - \boldsymbol{\rho}_{g,h}^\varepsilon)\|_{l^2} + |C_h - 1| \|\delta_+ (\Pi_h \rho_g^\varepsilon)\|_{l^2} \lesssim h. \tag{3.36}$$

∎

Remark 3.4. If we further assume that $|\rho_g^\varepsilon|_{H^2}$ is bounded, we can expect $\|\mathbf{e}_h^\varepsilon\|_{l^2} \lesssim h^2$ by the Bramble–Hilbert lemma and a standard scaling argument.

Finally, we study the convergence of $\boldsymbol{\rho}_{g,h}^\varepsilon$ as $\varepsilon \to 0^+$ with a fixed h and the result is summarized as follows.

THEOREM 3.5. *When $\beta \geq 0$ and $\delta \geq 0$, we have that*

$$\lim_{\varepsilon \to 0^+} \boldsymbol{\rho}_{g,h}^\varepsilon = \boldsymbol{\rho}_{g,h}^0, \tag{3.37}$$

where $\boldsymbol{\rho}_{g,h}^0$ is the ground state of $E_h^\varepsilon(\cdot)$ (3.6) with $\varepsilon = 0$.

Proof. The compactness of the finite-dimensional feasible set W_h (3.4) implies that, for any sequence $\varepsilon_n \to 0$, there exists a subsequence, denoted as the sequence itself for simplicity, such that $\lim_{n\to\infty} \boldsymbol{\rho}_{g,h}^{\varepsilon_n} = \tilde{\boldsymbol{\rho}}_h$ for some $\tilde{\boldsymbol{\rho}}_h \in W_h$. Consequently, $\lim_{n\to\infty} E_h^{\varepsilon_n}(\boldsymbol{\rho}_{g,h}^{\varepsilon_n}) = E_h^0(\tilde{\boldsymbol{\rho}}_h)$.

On the other hand, for any ε, we have $E_h^\varepsilon(\boldsymbol{\rho}_{g,h}^\varepsilon) \leq E_h^\varepsilon(\boldsymbol{\rho}_{g,h}^0) \leq E_h^0(\boldsymbol{\rho}_{g,h}^0)$, which indicates that $E_h^0(\tilde{\boldsymbol{\rho}}_h) \leq E_h^0(\boldsymbol{\rho}_{g,h}^0)$. Therefore, we must have $\tilde{\boldsymbol{\rho}}_h = \boldsymbol{\rho}_{g,h}^0$ due to the uniqueness of the ground state. Noticing that the above argument holds true for any sequence $\varepsilon_n \to 0$, we get the conclusion (3.37). ∎

The main works in sections 2 and 3 can be summarized in the following diagram. Since it is difficult to study the convergence of $\boldsymbol{\rho}_{g,h}^0$ to ρ_g directly, as indicated by the dashed arrow in the diagram, we study an approximating problem, i.e., the convergence of $\boldsymbol{\rho}_{g,h}^\varepsilon$ to ρ_g, which is indicated by the double arrow in the diagram. As shown in the diagram, we have studied it in two steps, namely, the convergence of $\boldsymbol{\rho}_{g,h}^\varepsilon$ to ρ_g^ε as $h \to 0^+$ (or $N \to \infty$), which has been proved in Theorem 3.3, and the convergence of ρ_g^ε to ρ_g as $\varepsilon \to 0^+$, which has been studied in Theorems 2.6 and 2.8. Though not related to our main problem, the convergence of $\boldsymbol{\rho}_{g,h}^\varepsilon$ to $\boldsymbol{\rho}_{g,h}^0$ has been studied as well in Theorem 3.5.

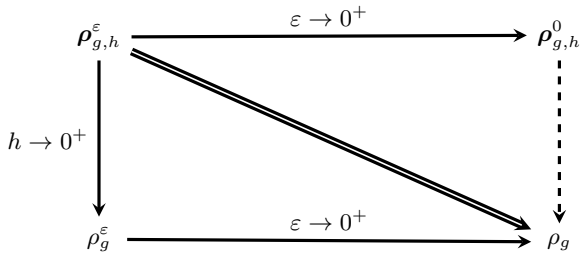

4. An accelerated projected gradient method. Numerous optimization techniques have been developed for solving a constrained convex optimization problem like (3.7). Among them, the APG method has been widely used due to its efficiency and easy implementation. For completeness, a brief introduction of the method is reviewed in this section.

The APG method is a special case of the accelerated proximal method, which is a generic method proposed in [12, 36] to solve problems of the type

$$\min_{\mathbf{u}\in\mathbb{R}^n} F(\mathbf{u}) := f(\mathbf{u}) + g(\mathbf{u}) \tag{4.1}$$

with $f(\mathbf{u})$ being convex and of type $C^{1,1}$, i.e., continuously differentiable with Lipschitz continuous gradient, and $g(\mathbf{u})$ being convex, simple, but possibly nonsmooth.

For the function g, being simple means easy computation of the proximal operation of g, i.e.,

$$\text{prox}_g(\mathbf{w}) := \arg\min_{\mathbf{u}\in\mathbb{R}^n} \left(g(\mathbf{u}) + \frac{1}{2}\|\mathbf{u}-\mathbf{w}\|_{l^2}^2 \right) \tag{4.2}$$

for any given $\mathbf{w} \in \mathbb{R}^n$. When $g(\mathbf{u}) = \mathbb{I}_Q(\mathbf{u})$, where $\mathbb{I}_Q(\cdot)$ is the indicator function defined as

$$\mathbb{I}_Q(\mathbf{u}) = \begin{cases} 0 & \text{if } \mathbf{u} \in Q, \\ \infty & \text{otherwise} \end{cases} \tag{4.3}$$

for some convex set Q, the accelerated proximal method becomes the APG method since now the operator $\text{prox}_g(\mathbf{w})$ becomes the l^2-projection of $\mathbf{w}$ onto Q, i.e.,

$$\text{prox}_g(\mathbf{w}) = \text{proj}_Q(\mathbf{w}) := \arg\min_{\mathbf{u}\in Q} \|\mathbf{u}-\mathbf{w}\|_{l^2}^2. \tag{4.4}$$

The problem (3.7) can be reformulated easily into the form (4.1) by taking

$$f(\boldsymbol{\rho}_h) = E_h^\varepsilon(\boldsymbol{\rho}_h), \quad g(\boldsymbol{\rho}_h) = \mathbb{I}_{W_h}(\boldsymbol{\rho}_h), \tag{4.5}$$

where $\boldsymbol{\rho}_h \in \mathbb{R}^{N-1}$ and $W_h \subset \mathbb{R}^{N-1}$ is the feasible set defined as (3.4). However, a further modification of $E_h^\varepsilon(\cdot)$ is necessary as follows:

$$\tilde{E}_h^\varepsilon(\boldsymbol{\rho}_h) = h\sum_{j=0}^{N-1} \left[\frac{1}{4}\frac{|\delta_x^+\rho_j|^2}{|\rho_j|+|\rho_{j+1}|+2\varepsilon} + V(x_j)|\rho_j| + \frac{\beta}{2}\rho_j^2 + \frac{\delta}{2}\left|\delta_x^+\rho_j\right|^2 \right]. \tag{4.6}$$

Here we impose the absolute sign on ρ_j to extend the domain of $E_h^\varepsilon(\cdot)$ from the feasible set W_h to the whole space $\mathbb{R}^{N-1}$ in order to apply the APG method. This modification is necessary to avoid possible breakdown of the optimization process. Denote

$$\tilde{\mathbf{g}}_h^\varepsilon(\boldsymbol{\rho}_h) = \left(\frac{\partial \tilde{E}_h^\varepsilon}{\partial \rho_1}, \frac{\partial \tilde{E}_h^\varepsilon}{\partial \rho_2}, \ldots, \frac{\partial \tilde{E}_h^\varepsilon}{\partial \rho_{N-1}} \right)^T. \tag{4.7}$$

Now its jth component becomes

$$\tilde{\mathbf{g}}_h^\varepsilon[j] := \frac{\partial \tilde{E}_h^\varepsilon}{\partial \rho_j} = h\left[-\frac{\delta_x^+ \tilde{f}_{j-1}}{2} - \frac{\tilde{f}_{j-1}^2 + \tilde{f}_j^2}{4} s_j + V(x_j)s_j + \beta\rho_j - \delta(\delta_x^2\rho_j) \right], \tag{4.8}$$

where

$$s_j = \text{sign}(\rho_j), \quad \tilde{f}_j = \tilde{f}_j(\boldsymbol{\rho}_h) := \frac{\delta_x^+\rho_j}{|\rho_j|+|\rho_{j+1}|+2\varepsilon} \quad \text{for } j = 0, 1, \ldots, N-1. \tag{4.9}$$

Obviously, for any $\boldsymbol{\rho}_h \in W_h$ (3.4), we have

$$\tilde{E}_h^\varepsilon(\boldsymbol{\rho}_h) = E_h^\varepsilon(\boldsymbol{\rho}_h), \quad \tilde{\mathbf{g}}_h^\varepsilon(\boldsymbol{\rho}_h) = \mathbf{g}_h^\varepsilon(\boldsymbol{\rho}_h), \tag{4.10}$$

and the minimizers of $\tilde{E}_h^\varepsilon(\cdot)$ in $\mathbb{R}^{N-1}$ lie in the feasible set W_h (3.4) or $-W_h$.

In practice, the fact that $g(\mathbf{u})$ is simple is crucial for the efficiency of the APG method since the evaluation of the proximal operator of $g(\cdot)$ is done at each iteration

and makes up the most time-consuming part in the optimization process. Therefore, it is necessary to check whether the function $\mathbb{I}_{W_h}(\boldsymbol{\rho}_h)$ is simple or not. Luckily, the feasible set W_h is a simplex and the projection onto W_h can be efficiently computed with an average computational cost $O(N \log N)$ or even $O(N)$ [17, 27, 37].

Now we are ready to show the detailed scheme for optimizing (4.6). The general framework comes from FISTA, a simple and popular APG method proposed in [12]. For simplicity, we introduce the following two notations: $Q_L(\mathbf{u}, \boldsymbol{\rho}_h)$ and $p_L(\boldsymbol{\rho}_h)$. For given $L > 0$, $\mathbf{u} \in \mathbb{R}^{N-1}$, and $\boldsymbol{\rho}_h \in \mathbb{R}^{N-1}$, we denote

$$Q_L(\mathbf{u}, \boldsymbol{\rho}_h) = \tilde{E}_h^\varepsilon(\boldsymbol{\rho}_h) + (\mathbf{u} - \boldsymbol{\rho}_h)^T \tilde{\mathbf{g}}_h^\varepsilon(\boldsymbol{\rho}_h) + \frac{L}{2}\|\mathbf{u} - \boldsymbol{\rho}_h\|_2^2 + \mathbb{I}_{W_h}(\mathbf{u}) \tag{4.11}$$

and

$$p_L(\boldsymbol{\rho}_h) := \arg\min_{\mathbf{u} \in \mathbb{R}^{N-1}} Q_L(\mathbf{u}, \boldsymbol{\rho}_h). \tag{4.12}$$

Obviously, $Q_L(\cdot, \boldsymbol{\rho}_h)$ is a quadratic approximation of $\tilde{E}_h^\varepsilon(\cdot) + \mathbb{I}_{W_h}(\cdot)$ near $\boldsymbol{\rho}_h$, and $p_L(\boldsymbol{\rho}_h)$, the minimizer of $Q_L(\cdot, \boldsymbol{\rho}_h)$, exists and is unique for any given $\boldsymbol{\rho}_h$. Furthermore, a simple algebra shows that

$$\begin{aligned} p_L(\boldsymbol{\rho}_h) &= \arg\min_{\mathbf{u} \in W_h} \left\| \mathbf{u} - \left(\boldsymbol{\rho}_h - \frac{1}{L} \tilde{\mathbf{g}}_h^\varepsilon(\boldsymbol{\rho}_h) \right) \right\|_{l^2}^2 \\ &= \mathrm{proj}_{W_h} \left(\boldsymbol{\rho}_h - \frac{1}{L} \tilde{\mathbf{g}}_h^\varepsilon(\boldsymbol{\rho}_h) \right), \end{aligned} \tag{4.13}$$

i.e., $p_L(\boldsymbol{\rho}_h)$ is the projection of $\boldsymbol{\rho}_h - \frac{1}{L}\tilde{\mathbf{g}}_h^\varepsilon(\boldsymbol{\rho}_h)$ onto the feasible set W_h (3.4). With all these preparations, we are ready to show the detailed algorithm in Algorithm 4.1. As shown in [12], we have $E_h^\varepsilon(\boldsymbol{\rho}_h^{(k)}) - E_h^\varepsilon(\boldsymbol{\rho}_h^{(k+1)}) \lesssim \mathcal{O}(1/k^2)$, where $\boldsymbol{\rho}_h^{(k)}$ is the vector computed after k iterations. In other words, a quadratic convergence rate in energy could be expected.

We remark here that there have been many efficient MATLAB packages developed for the problem (4.1) based on APG, such as TFOCS [13]. These packages, which are based on similar ideas to FISTA, are usually more efficient and robust, though more complicated, than FISTA. Therefore, these packages could be used to replace FISTA in the Algorithm 4.1 for a better numerical performance.

Remark 4.1. The approximate ground states obtained in [42] for different parameter regimes can be taken as good a initial guess in the rDF-APG method.

Remark 4.2. The two-grid technique, where we start from a coarse mesh and make the refined solution on the coarse mesh to be the initial guess for the fine mesh, will be useful to speed up the algorithm. Similarly, when ε is small, it is useful to apply the continuation technique, which means we start with a relatively large ε and use the result as the initial guess for a smaller ε.

Remark 4.3. Based on our numerical experiments not reported here for brevity, we observed that when ε is extremely small, it is better to choose η in Algorithm 4.1 close to 1.

Remark 4.4. Numerical experiments suggest that a further regularization could lead to a much better numerical performance. With the regularization, we get the following new regularized energy functional

$$\hat{E}^\varepsilon(\rho) = \int_{\mathbb{R}^d} \left[\frac{|\nabla\rho|^2}{8(|\rho| + \varepsilon)} + V(\mathbf{x}) \left(\sqrt{\rho^2 + \varepsilon^2} - \varepsilon \right) + \frac{\beta}{2}\rho^2 + \frac{\delta}{2}|\nabla\rho|^2 \right] d\mathbf{x}, \tag{4.14}$$

Algorithm 4.1 rDF-APG: Optimize (4.6) via FISTA.

Choose a sufficiently small $\varepsilon > 0$ and a proper initial guess $\boldsymbol{\rho}_h^{(0)}$.
Choose $L_0 > 0$, $\eta > 1$.
$k \leftarrow 1$, $t_1 \leftarrow 1$, $\mathbf{y}_1 \leftarrow \boldsymbol{\rho}_h^{(0)}$, $\bar{L} \leftarrow L_0$
$\tilde{\boldsymbol{\rho}}_h \leftarrow p_{\bar{L}}(\mathbf{y}_1)$
while $k = 1$ or $\|\boldsymbol{\rho}_h^{(k-1)} - \boldsymbol{\rho}_h^{(k-2)}\|_{l^2} >$ tolerence **do**
  while $E_h^\varepsilon(\tilde{\boldsymbol{\rho}}_h) > Q_{\bar{L}}(\tilde{\boldsymbol{\rho}}_h, \mathbf{y}_k)$ **do**
    $\bar{L} \leftarrow \eta\bar{L}$, $\tilde{\boldsymbol{\rho}}_h \leftarrow p_{\bar{L}}(\mathbf{y}_k)$
  end while
  $\boldsymbol{\rho}_h^{(k)} \leftarrow \tilde{\boldsymbol{\rho}}_h$, $t_{k+1} \leftarrow \frac{1+\sqrt{1+4t_k^2}}{2}$, $L_k \leftarrow \bar{L}$
  $\mathbf{y}_{k+1} \leftarrow \boldsymbol{\rho}_h^{(k)} + \left(\frac{t_k - 1}{t_{k+1}}\right)(\boldsymbol{\rho}_h^{(k)} - \boldsymbol{\rho}_h^{(k-1)})$
  $k \leftarrow k + 1$
end while
$\boldsymbol{\rho}_{g,h}^\varepsilon \leftarrow \boldsymbol{\rho}_h^{(k-1)}$

where $\rho \in W$ (2.3). Obviously, $\hat{E}^\varepsilon(\cdot)$ is convex in W (2.3). Denote $\hat{\rho}_g^\varepsilon$ to be the ground state of $\hat{E}^\varepsilon(\cdot)$, which is defined as

$$\hat{\rho}_g^\varepsilon = \arg\min_{\rho \in W} \hat{E}^\varepsilon(\rho). \tag{4.15}$$

It can be shown that Theorems 2.4, 2.6, and 2.8 still hold true if we replace ρ_g^ε by $\hat{\rho}_g^\varepsilon$ in the theorems. A detailed description of its finite difference discretization can be found in Appendix A.

5. Numerical results. In this section, we illustrate the performance of the rDF-APG method proposed in this paper. In particular, we will verify the spatial accuracy result in Theorem 3.3 and test the convergence of ρ_g^ε as $\varepsilon \to 0^+$. Besides, we compare the rDF-APG method with the regularized Newton method [44] to show the great advantage of our method when the HOI effect is dominant. Applications of our method to multidimensional problems are also reported. As a remark, all the problems in this section are formulated via $\hat{E}^\varepsilon(\cdot)$ (4.14) and all numerical ground state densities are denoted as $\boldsymbol{\rho}_{g,h}^\varepsilon$ for simplicity.

5.1. Spatial accuracy. To check the spatial accuracy of the ground state $\boldsymbol{\rho}_{g,h}^\varepsilon$ defined in (3.7), we fix $\varepsilon > 0$. For simplicity, only the following 1-dimensional case in Example 5.1 is considered. For multidimensional problems, the results are similar.

Example 5.1. Consider the external potential to be $V(x) = x^2/2$ and the computational domain $\Omega = (-M, M)$ with M sufficiently large. The two nonnegative parameters β and δ can be chosen arbitrarily. In particular, we consider the following two cases with $M = 16$:

- Case I: $\beta = 10$ and $\delta = 0$.
- Case II: $\beta = 10$ and $\delta = 10$.

Obviously, there is no HOI effect in Case I.

For the fixed $\varepsilon = 10^{-3}$, the "exact" ground state density ρ_g^ε for Cases I and II in Example 5.1 can be accurately approximated via the rDF-APG method with an extremely small mesh size, say $h = \frac{1}{4096}$, and an extremely small tolerance, say 10^{-12}. If we denote the corresponding energy as $E_{\rm ex}^\varepsilon := E^\varepsilon(\rho_g^\varepsilon)$, it can be computed that $E_{\rm ex}^\varepsilon \approx 1.927$ in Case I and $E_{\rm ex}^\varepsilon \approx 2.207$ in Case II.

TABLE 1

Spatial accuracy of rDF-APG for Case I *in Example* 5.1. *In the table, we denote* $\mathbf{e}_h^\varepsilon := \Pi_h \rho_g^\varepsilon - \boldsymbol{\rho}_{g,h}^\varepsilon$, *where* $\Pi_h \rho_g^\varepsilon$ *is defined in* (3.27).

Error	$h = 1/2$	$h/2$	$h/2^2$	$h/2^3$	$h/2^4$	$h/2^5$
$\lvert E_{g,h}^\varepsilon - E_{\rm ex}^\varepsilon\rvert$	7.74E-3	1.97E-3	4.93E-4	1.23E-4	3.06E-5	7.59E-6
rate	-	**1.98**	**2.00**	**2.00**	**2.01**	**2.01**
$\lVert \mathbf{e}_h^\varepsilon\rVert_{l^2}$	1.17E-1	2.97E-2	7.45E-3	1.84E-3	4.48E-4	8.74E-5
rate	-	1.98	2.00	2.01	2.04	2.36
$\lVert \delta_+ \mathbf{e}_h^\varepsilon\rVert_{l^2}$	2.18E-3	1.07E-3	5.33E-4	2.66E-4	1.33E-4	6.65E-5
rate	-	**1.02**	**1.01**	**1.00**	**1.00**	**1.00**
$\lVert \mathbf{e}_h^\varepsilon\rVert_{l_\infty}$	5.12E-3	1.29E-3	3.27E-4	8.10E-5	1.98E-5	3.73E-6
rate	-	1.99	1.98	2.01	2.03	2.41

TABLE 2

Spatial accuracy of rDF-APG for Case II *in Example* 5.1. *In the table, we denote* $\mathbf{e}_h^\varepsilon := \Pi_h \rho_g^\varepsilon - \boldsymbol{\rho}_{g,h}^\varepsilon$, *where* $\Pi_h \rho_g^\varepsilon$ *is defined in* (3.27).

Error	$h = 1/2$	$h/2$	$h/2^2$	$h/2^3$	$h/2^4$	$h/2^5$
$\lvert E_{g,h}^\varepsilon - E_{\rm ex}^\varepsilon\rvert$	9.07E-3	2.28E-3	5.73E-4	1.43E-4	3.56E-5	8.81E-6
rate	-	**1.99**	**1.99**	**2.00**	**2.01**	**2.01**
$\lVert \mathbf{e}_h^\varepsilon\rVert_{l^2}$	5.98E-2	1.44E-2	3.59E-3	8.88E-4	2.19E-4	4.91E-5
rate	-	2.06	2.00	2.02	2.02	2.16
$\lVert \delta_+ \mathbf{e}_h^\varepsilon\rVert_{l^2}$	1.43E-3	7.10E-4	3.54E-4	1.77E-4	8.85E-5	4.42E-5
rate	-	**1.01**	**1.00**	**1.00**	**1.00**	**1.00**
$\lVert \mathbf{e}_h^\varepsilon\rVert_{l_\infty}$	2.33E-3	6.01E-4	1.51E-4	3.77E-5	9.35E-6	2.14E-6
rate	-	1.95	2.00	2.00	2.01	2.13

Tables 1 and 2 show the spatial accuracy of $\boldsymbol{\rho}_{g,h}^\varepsilon$ for Cases I and II in Example 5.1, respectively. From the tables, we can observe the second order accuracy of energy and first order accuracy of $\delta_+ \boldsymbol{\rho}_{g,h}^\varepsilon$ in the l^2-norm, which are consistent with Theorem 3.3. In fact, Tables 1 and 2 show something more than expected. First, we observe a roughly second order accuracy in the l^2-norm of $\boldsymbol{\rho}_{g,h}^\varepsilon$ while only the first order accuracy can be proved in Theorem 3.3. One possible explanation is that the ground state is regular and thus we can get a higher order accuracy noticing Remark 3.4. Besides, it seems that we still have the first order accuracy of $\delta_+ \boldsymbol{\rho}_{g,h}^\varepsilon$ in the l^2-norm when $\delta = 0$, although we can no longer prove such a result following a similar procedure to that in Theorem 3.3.

5.2. Convergence of ground states. To verify numerically the convergence of the ground state densities of the regularized energy functionals, we choose a sequence $\{\varepsilon_n\}$ such that $\lim_{n\to\infty} \varepsilon_n = 0$. For each ε_n, we choose a sufficiently small mesh size to make the spatial error negligible. In general, the smaller ε is, the finer mesh that is needed.

Here we consider the 1-dimensional example as shown in Case II of Example 5.1. Denote ρ_g^ε to be the exact ground state density for the fixed $\varepsilon > 0$, which is numerically computed via the rDF-APG method, and ρ_g to be the exact numerical ground state density of the original energy functional (2.1), i.e., when $\varepsilon = 0$, which is approximated by ρ_g^ε with a sufficiently small ε, say $\varepsilon = 10^{-8}$. Figure 1 shows the ground state densities computed for different $\varepsilon \geq 0$. It can be observed that ρ_g^ε is less concentrated than ρ_g, but will converge to ρ_g as $\varepsilon \to 0^+$. More detailed comparisons are made in Table 3. From Table 3, we find that ρ_g^ε and $E^\varepsilon(\rho_g^\varepsilon)$ converge to ρ_g and $E(\rho_g)$, respectively, almost linearly with respect to the regularization parameter $0 < \varepsilon \ll 1$.

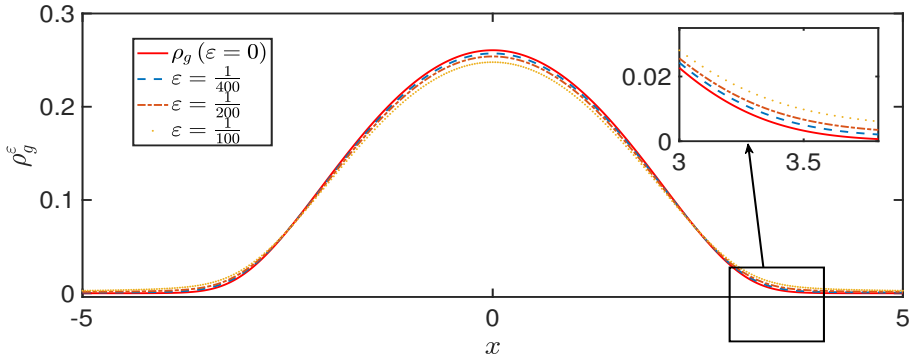

FIG. 1. *Comparison of* ρ_g^ε (2.5) *computed via the rDF-APG method and the exact ground state density* ρ_g (2.2) *for Case* II *in Example* 5.1.

TABLE 3
Convergence test of the ground state densities as $\varepsilon \to 0^+$ *for Case* II *in Example* 5.1.

ε	10^{-1}	10^{-2}	10^{-3}	10^{-4}	10^{-5}	10^{-6}
$\lvert E^\varepsilon(\rho_g^\varepsilon) - E(\rho_g)\rvert$	1.04E0	2.04E-1	2.84E-2	3.70E-3	4.56E-4	5.62E-5
rate	-	0.71	0.86	0.88	0.90	0.92
$\lVert\rho_g^\varepsilon - \rho_g\rVert_2$	1.54E-1	2.45E-2	2.73E-3	2.95E-4	3.08E-5	3.08E-6
rate	-	0.80	0.95	0.97	0.98	1.00
$\lVert\rho_g^\varepsilon - \rho_g\rVert_\infty$	8.64E-2	1.28E-2	1.43E-3	1.54E-4	1.52E-5	1.70E-6
rate	-	0.83	0.95	0.97	1.00	0.95

TABLE 4
Effect of ε *on the efficiency of the rDF-APG method. In the numerical test, we choose* $\beta = 10$, $\delta = 100$, $h = \frac{1}{64}$, $\Omega = (-16, 16)$, *and a very small tolerance* 10^{-10}. *The two-grid technique is applied to speed up. The result is accurate to the first digit. The method fails when* $\varepsilon = 0$.

ε	10^{-2}	10^{-4}	10^{-6}	10^{-8}	0
CPU time	5.7s	18.3s	60.7s	159.4s	N.A.

The computational cost is highly related to the value of ε. For Case II of Example 5.1, numerical experiments indicate that it would be difficult to make $\|\boldsymbol{\rho}_h^{(k+1)} - \boldsymbol{\rho}_h^{(k)}\|_{l^2}$ converge within a very small tolerance, say 10^{-10}, when ε is extremely small, say $\varepsilon \ll 10^{-8}$, where $\boldsymbol{\rho}_h^{(k)}$ is the intermediate state computed after k iterations. The relatively slow convergence of the intermediate states $\boldsymbol{\rho}_h^{(k)}$ when ε is extremely small is the main drawback of our method. Numerical evidence is shown in Table 4, from which we can clearly observe the increasing computational cost as $\varepsilon \to 0$. In particular, the method fails when $\varepsilon = 0$. On the other hand, though not explicitly shown here for brevity, numerical experiments indicate that our method works well if we are only concerned with the ground state energy, even when ε is very small, since we can choose a relatively larger tolerance to have a much faster convergence.

5.3. Effect of interaction strength. The contact interaction strength β and the HOI strength δ affect the ground state in different ways. As an example, we consider the problem defined in the whole space under the harmonic potential $V(x) = \frac{x^2}{2}$. In Figure 2, (a) and (b) show the ground state densities with different choices of β and δ. As shown in the figure, both the strong contact interaction and the strong

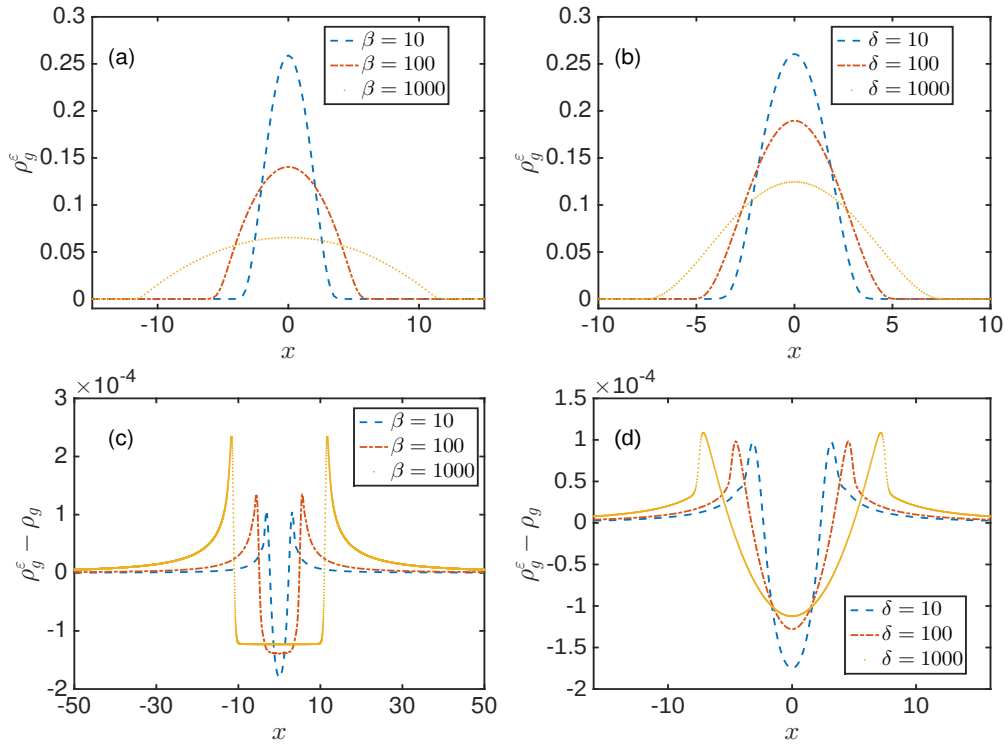

FIG. 2. *Ground state density* ρ_g^ε (2.5) *(top row, i.e.,* (a), (b)*) and its comparison with* ρ_g (2.2) *(bottom row, i.e.,* (c), (d)*) with* $\delta = 10$ *and different* β*'s (left column, i.e.,* (a), (c)*) or* $\beta = 10$ *and different* δ*'s (right column, i.e.,* (b), (d)*). Here we choose* $\varepsilon = 10^{-4}$.

HOI effect will spread the ground state, but in different ways. The detailed limiting Thomas–Fermi approximations of the ground states could be referred to [7, 42]. The subfigures (c) and (d) in Figure 2 show explicitly how the values of β and δ are related to the difference $\rho_g^\varepsilon - \rho_g$. Comparing this with (a) and (b) in Figure 2, when $\beta \gg 1$, the difference will almost be a constant in the region where ρ_g is obviously bigger than 0. When $\delta \gg 1$, the pattern of the difference will be different. In fact, by considering the Euler–Lagrange equation satisfied by ρ_g and ρ_g^ε, we can show that the difference in this case is roughly a quadratic function in the region where ρ_g is obviously bigger than 0.

The strength of interaction would affect the numerical performance of the rDF-APG method as well. We expect that the rDF-APG method works better when the interaction is stronger since the interaction energy terms are quadratic with respect to the density function formulation, which is the ideal form for most optimization techniques. As a result, we can expect a great advantage of the rDF-APG method over methods based on the wave function formulation when the interaction energy part, especially the HOI part, is dominant. To better illustrate the advantage of the density function formulation we introduced, we compare the rDF-APG method with the regularized Newton method [41, 44], which is one of the state-of-the-art numerical methods for computing ground states of BEC [44]. In fact, both methods share a similar strategy in designing the numerical methods, i.e., first discretize the energy functional to get a finite-dimensional constrained optimization problem and then adapt modern optimization techniques to compute the ground state. The dif-

TABLE 5

CPU time by using the rDF-APG and the regularized Newton methods. In the numerical test, we choose $h = \frac{1}{64}$ *and the computation domain to be* $(-32, 32)$*. For the rDF-APG method, we choose* $\varepsilon = 10^{-4}$*,* $tol = 10^{-8}$ *and apply the two-grid technique to speed up. All numerical experiments are performed on the same laptop. The CPU time shown in the table is accurate to the first digit.*

	rDF-APG				Regularized Newton method			
δ \ β	10	10^2	10^3	10^4	10	10^2	10^3	10^4
10	18.34 s	12.39 s	4.29 s	1.67 s	4.54 s	3.76 s	3.47 s	3.85 s
10^2	10.66 s	8.66 s	3.78 s	1.58 s	18.79 s	13.42 s	9.36 s	7.62 s
10^3	5.25 s	6.29 s	3.66 s	1.67 s	116.65 s	79.41 s	45.49 s	34.03 s
10^4	3.31 s	3.60 s	3.03 s	1.66 s	224.05 s	222.71 s	224.89 s	144.14 s

ference is that the regularized Newton method adopts the wave function formulation while the rDF-APG method uses the density function formulation. We choose all the setup of the problem, including the initial data and the stopping criteria, to be exactly the same for a fair comparison. The initial guess is chosen to be of Gaussian-type and the stopping tolerance is chosen to be 10^{-8}. All the other parameters in the regularized Newton method are chosen to be the default ones. For the rDF-APG method, we fix $\varepsilon = 10^{-4}$ and choose $\eta = 1/0.9$. We run the two methods on the same laptop and the CPU time for different cases are shown in Table 5. Although the CPU time will not be exactly the same for each run, the results shown in the table are computed by averaging, which are accurate to the first digit and enough to verify our expectations. As shown in the table, the advantage of the rDF-APG method over the regularized Newton method is not obvious when β and δ are small. However, when one of β and δ is large, especially when the δ term is dominant, there is a huge difference between the regularized Newton method and the rDF-APG method considering computational cost. What's more, the stronger the interaction is, the faster the rDF-APG method becomes, which is completely different from the regularized Newton method. As a conclusion, the rDF-APG method works for all positive β and δ, and is extremely suitable for cases with strong interaction effect.

5.4. Numerical examples in high dimensions. The rDF-APG methd can be easily adapted to multidimensional problems with tensor grids. In this section, we show examples in two dimensions (2D) and three dimensions (3D) to indicate the feasibility of our method for multidimensional problems.

Consider a box potential,

$$V(\mathbf{x}) = \begin{cases} 0, & \mathbf{x} \in \Omega \subset \mathbb{R}^d, \\ \infty, & \mathbf{x} \in \Omega^c. \end{cases} \tag{5.1}$$

In 2D, we take $\Omega = (-1, 1)^2$. The numerical ground state densities with $\varepsilon = 10^{-4}$ and different choices of β and δ are shown in Figure 3. We observe the ground state becomes almost a constant inside the domain when $\beta \gg 1$, while the ground state converges to another pattern when $\delta \gg 1$.

In 3D, we take $\Omega = (-1, 1)^3$. Figure 4 shows the isosurface end-cap geometry of the ground state with different values of β and δ. As shown in the figure, again we can conclude that the solution spreads in a similar way to the 2D case shown in Figure 3 when β or δ increases since the slices in Figure 4 shows a similar pattern.

Next, we consider the whole space problem under an optical potential,

$$V(x, y, z) = \frac{x^2 + 4y^2 + 4z^2}{2} + A(\sin^2(x) + \sin^2(y) + \sin^2(z)). \tag{5.2}$$

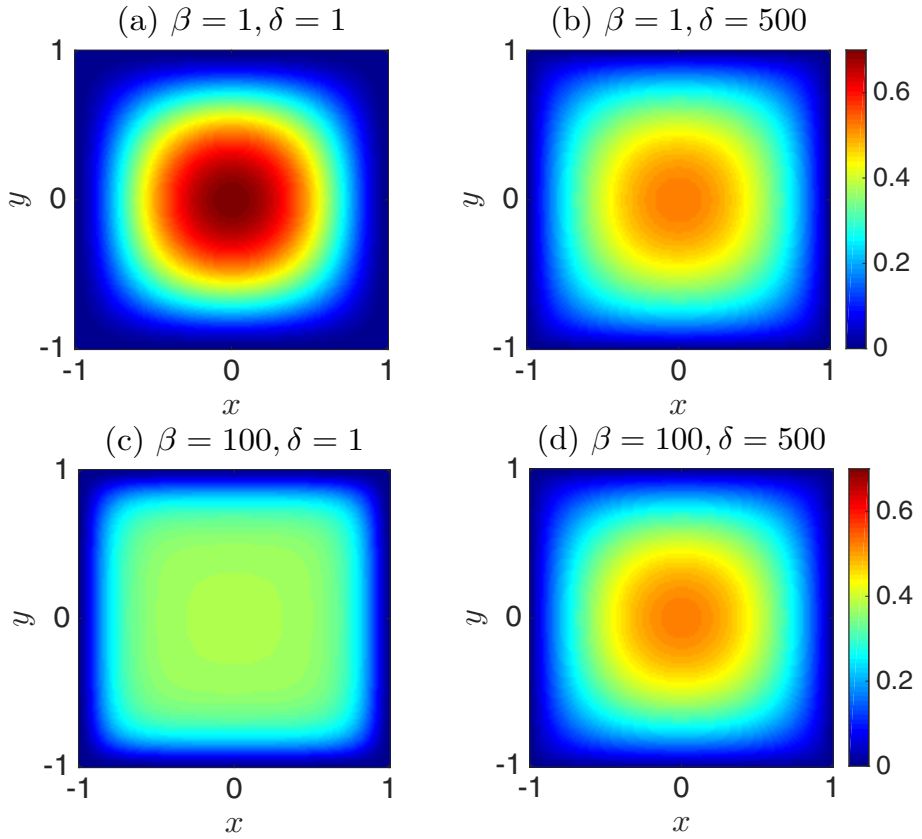

FIG. 3. *Ground state densities* $\rho_g^\varepsilon(x, y)$ *with* $\beta = 1{,}100$ *(from top to bottom) and* $\delta = 1{,}500$ *(from left to right) under the box potential in* $\Omega = (-1, 1)^2$. *Here we choose* $\varepsilon = 10^{-4}$.

Obviously, when $A = 0$, we get the harmonic potential. Figure 5 shows the isosurface of the numerical ground state densities with $\varepsilon = 10^{-4}$, $A = 20$, and different values of β and δ. The ground state densities shown in Figure 5 are consistent with the results shown in [40]. Again we observe that the ground state densities become less concentrated as β or δ increases.

6. Conclusion. We proposed the rDF-APG method, which computes the ground state density of the MGPE by directly minimizing the regularized energy functional formulated via the density function and discretized via the finite difference method. The convergence of the ground state densities as the regularization effect vanishes was rigorously proved. The detailed finite difference discretization was provided, with its spatial accuracy analyzed. Numerical experiments verified the spatial accuracy of the numerical ground state density computed via the rDF-APG method as well as its convergence as $\varepsilon \to 0^+$. Furthermore, we studied the effect of the interaction strength on the ground state density as well as on the performance of the rDF-APG method. In particular, we showed the advantage of our method concerning the computational cost when the interaction, especially the HOI effect, is strong.

Appendix A. A finite difference discretization of $\hat{E}^\varepsilon(\cdot)$. Numerical experiments suggest that a further regularization of the external potential term should

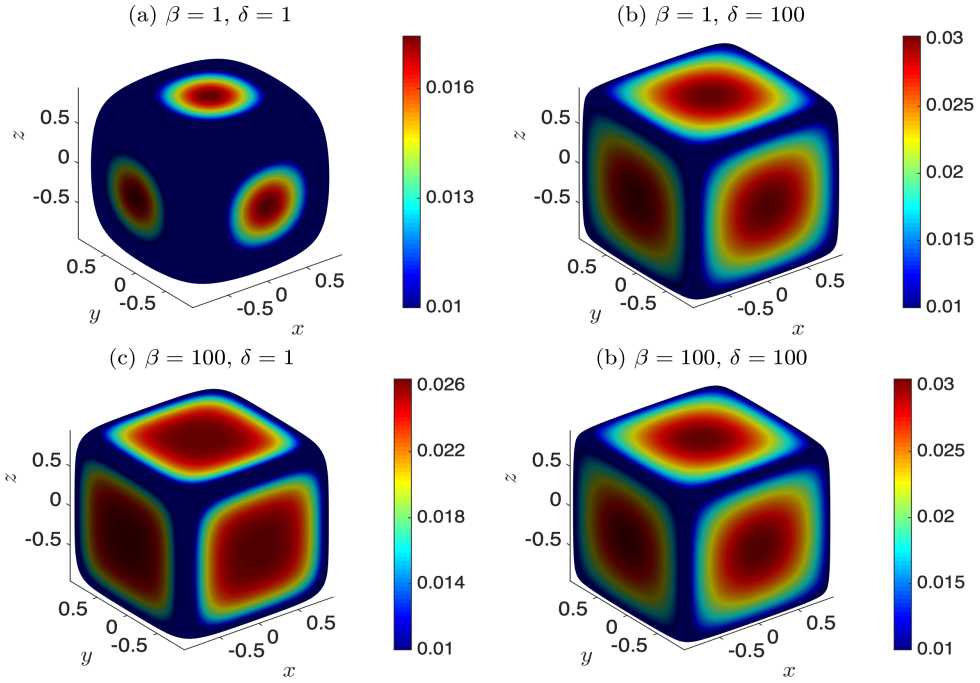

FIG. 4. *Isosurface (isovalues* 0.01*) of the ground state densities* $\rho_g^\varepsilon(x, y, z)$ *with an end cap. The external potential is chosen to be a box potential in* $(-1, 1)^3$ *and we choose* $\varepsilon = 10^{-4}$.

be applied, and the new regularized energy functional $\hat{E}^\varepsilon(\cdot)$ (4.14) has a much better numerical performance than $E^\varepsilon(\cdot)$ (2.4). Denote $\hat{E}_h^\varepsilon(\cdot)$ to be the finite difference discretization of $\hat{E}^\varepsilon(\cdot)$. For simplicity, only the 1-dimensional case is considered here. Following a similar procedure as in (3.5), we have

(A.1)
$$\hat{E}_h^\varepsilon(\boldsymbol{\rho}_h) = h \sum_{j=0}^{N-1} \left[\frac{1}{4} \frac{|\delta_x^+ \rho_j|^2}{|\rho_j| + |\rho_{j+1}| + 2\varepsilon} + V(x_j) \left(\sqrt{\rho_j^2 + \varepsilon^2} - \varepsilon \right) + \frac{\beta}{2} \rho_j^2 + \frac{\delta}{2} \left| \delta_x^+ \rho_j \right|^2 \right],$$

where $\rho_{j+\frac{1}{2}} := (\rho_j + \rho_{j+1})/2$. Similarly, we can compute its gradient. Denote

$$\hat{\mathbf{g}}_h^\varepsilon(\boldsymbol{\rho}_h) = \left(\frac{\partial \hat{E}_h^\varepsilon}{\partial \rho_1}, \frac{\partial \hat{E}_h^\varepsilon}{\partial \rho_2}, \ldots, \frac{\partial \hat{E}_h^\varepsilon}{\partial \rho_{N-1}} \right)^T. \tag{A.2}$$

Then its jth component can be explicitly computed as

$$\hat{\mathbf{g}}_h^\varepsilon[j] = h \left[-\frac{\delta_x^+ \tilde{f}_{j-1}}{2} - \frac{\tilde{f}_{j-1}^2 + \tilde{f}_j^2}{4} s_j + \frac{V(x_j)\rho_j}{\sqrt{\rho_j^2 + \varepsilon^2}} + \beta \rho_j - \delta(\delta_x^2 \rho_j) \right], \tag{A.3}$$

where s_j and $\tilde{f}_j$ were defined in (4.9). Comparing $\hat{\mathbf{g}}_h^\varepsilon[j]$ (A.3) and $\tilde{\mathbf{g}}_h^\varepsilon[j]$ (4.8), we observe that $\hat{\mathbf{g}}_h^\varepsilon[j]$ is more regular than $\tilde{\mathbf{g}}_h^\varepsilon[j]$, where $\rho_j \approx 0$ and $V(x_j) \gg 1$. The observation could possibly explain the better performance of the new formulation $\hat{E}_h^\varepsilon(\cdot)$ (A.1).

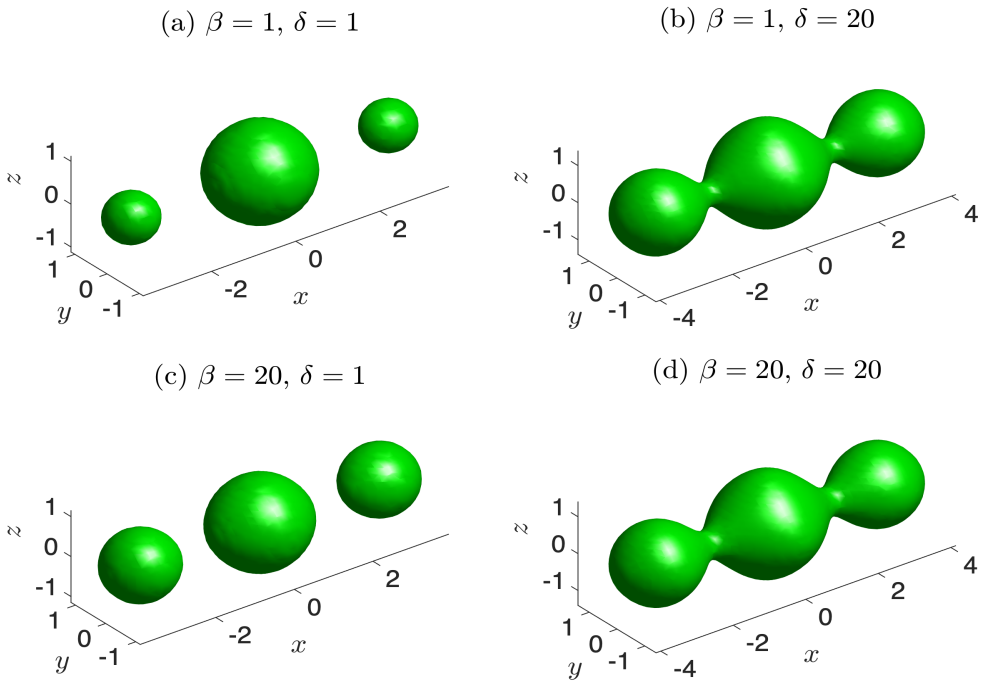

FIG. 5. *Isosurface of the numerical ground state densities* $\rho_g^\varepsilon(x, y, z)$ *with isovalues* 0.01. *The optical potential* (5.2) *is considered with* $A = 20$ *and different values of* β *and* δ. *Here we choose* $\varepsilon = 10^{-4}$.

Here we define $\hat{\boldsymbol{\rho}}_{g,h}^\varepsilon \in \mathbb{R}^{N-1}$ as follows:

$$\hat{\boldsymbol{\rho}}_{g,h}^\varepsilon = \arg\min_{\boldsymbol{\rho}_h \in W_h} \hat{E}_h^\varepsilon(\boldsymbol{\rho}_h). \tag{A.4}$$

Obviously, $\hat{\boldsymbol{\rho}}_{g,h}^\varepsilon$ is the numerical approximation of $\hat{\rho}_g^\varepsilon$ (4.15). Then it can be shown that Theorems 3.2, 3.3, and 3.5 still hold true if we replace $\boldsymbol{\rho}_{g,h}^\varepsilon$ by $\hat{\boldsymbol{\rho}}_{g,h}^\varepsilon$ in the theorems. The argument is almost exactly the same and thus omitted here for brevity.

REFERENCES

[1] M. H. Anderson, J. R. Ensher, M. R. Matthews, C. E. Wieman, and E. A. Cornell, *Observation of Bose-Einstein condensation in a dilute atomic vapor*, Science, 269 (1995), pp. 198–201.

[2] X. Antoine, A. Levitt, and Q. Tang, *Efficient spectral computation of the stationary states of rotating Bose-Einstein condensates by the preconditioned nonlinear conjugate gradient method*, J. Comput. Phys., 343 (2017), pp. 92–109.

[3] X. Antoine and R. Duboscq, *Robust and efficient preconditioned Krylov spectral solvers for computing the ground states of fast rotating and strongly interacting Bose-Einstein condensates*, J. Comput. Phys., 258 (2014), pp. 509-523.

[4] W. Bao, *Ground states and dynamics of multicomponent Bose–Einstein condensates*, Multiscale Model. Simul., 2 (2004), pp. 210–236.

[5] W. Bao, *Mathematical models and numerical methods for Bose-Einstein condensation*, in Proceedings of the International Congress of Mathematicians, Seoul, Korea, 2014, pp. 971–996.

[6] W. Bao and Y. Cai, *Mathematical theory and numerical methods for Bose–Einstein condensation*, Kinet. Relat. Models, 6 (2013), pp. 1–135.

[7] W. Bao, Y. Cai, and X. Ruan, *Ground states and dynamics of Bose-Einstein condensation with higher order interactions*, Phys. D, 386–387 (2019), pp. 38–48.
[8] W. Bao, Y. Cai, and H. Wang, *Efficient numerical methods for computing ground states and dynamics of dipolar Bose–Einstein condensates*, J. Comput. Phys., 229 (2010), pp. 7874–7892.
[9] W. Bao, I. L. Chern, and F. Y. Lim, *Efficient and spectrally accurate numerical methods for computing ground and first excited states in Bose–Einstein condensates*, J. Comput. Phys., 219 (2006), pp. 836–854.
[10] W. Bao and Q. Du, *Computing the ground state solution of Bose-Einstein condensates by a normalized gradient flow*, SIAM J. Sci. Comput., 25 (2004), pp. 1674–1697.
[11] W. Bao and W. Tang, *Ground-state solution of Bose-Einstein condensate by directly minimizing the energy functional*, J. Comput. Phys., 187 (2003), pp. 230–254.
[12] A. Beck and M. Teboulle, *A fast iterative shrinkage-thresholding algorithm for linear inverse problems*, SIAM J. Imaging Sci., 2 (2009), pp. 183–202.
[13] S. Becker, E. J. Candès, and M. Grant, *Templates for convex cone problems with applications to sparse signal recovery*, Math. Program. Comput., 3 (2011), pp. 165–218.
[14] R. Benguria, H. Brezis, and E. H. Lieb, *The Thomas-Fermi-von Weizsäcker theory of atoms and molecules*, Comm. Math. Phys., 79 (1981), pp. 167–180.
[15] C. C. Bradley, C. A. Sackett, J. J. Tollett, and R. G. Hulet, *Evidence of Bose-Einstein condensation in an atomic gas with attractive interactions*, Phys. Rev. Lett., 75 (1995), pp. 1687–1690.
[16] A. Braides, *A handbook of Γ-convegence*, in Handbook of Differential Equations: Stationary Partial Differential Equations, M. Chipot and P. Quittner, eds., Vol. 3, Elsevier, Amsterdam, 2006, pp. 101–213.
[17] P. Brucker, *An $o(n)$ algorithm for quadratic knapsack problems*, Oper. Res. Lett., 3 (1984), pp. 163–166.
[18] E. Cancès, G. Stoltz, and M. Lewin, *The electronic ground-state energy problem: A new reduced density matrix approach*, J. Chem. Phys., 125 (2006), 064101.
[19] I. Catto, C. Le Bris, and P.-L. Lions, *Mathematical Theory of Thermodynamic Limits: Thomas-Fermi Type Models*, Oxford University Press, Oxford, 1998.
[20] S.-M. Chang, W.-W. Lin, and S.-F. Shieh, *Gauss-Seidel-type methods for energy states of a multi-component Bose-Einstein condensate*, J. Comput. Phys., 202 (2005), pp. 367–390.
[21] C. Chin, R. Grimm, P. Julienne, and E. Tiesinga, *Feshbach resonances in ultracold gases*, Rev. Mod. Phys., 82 (2010), pp. 1225–1286.
[22] M. L. Chiofalo, S. Succi, and M. P. Tosi, *Ground state of trapped interacting Bose-Einstein condensates by an explicit imaginary-time algorithm*, Phys. Rev. E (3), 62 (2000), pp. 7438–7444.
[23] A. Collin, P. Massignan, and C. J. Pethick, *Energy-dependent effective interactions for dilute many-body systems*, Phys. Rev. A (3), 75 (2007), 013615.
[24] I. Danaila and B. Protas, *Computation of ground states of the Gross–Pitaevskii functional via Riemannian optimization*, SIAM J. Sci. Comput., 39 (2017), pp. B1102–B1129.
[25] K. B. Davis, M. O. Mewes, M. R. Andrews, N. J. van Druten, D. S. Durfee, D. M. Kurn, and W. Ketterle, *Bose-Einstein condensation in a gas of sodium atoms*, Phys. Rev. Lett., 75 (1995), pp. 3969–3973.
[26] C. D'Errico, M. Zaccanti, M. Fattori, G. Roati, M. Inguscio, G. Modugno, and A. Simoni, *Feshbach resonances in ultracold ^{39}K*, New J. Phys., 9 (2007), 223.
[27] J. Duchi, S. Shalev-Shwartz, Y. Singer, and T. Chandra, *Efficient projections onto the l^1-ball for learning in high dimensions*, in Proceedings of the International Conference on Machine Learning, Helsinki, Finland, 2008, International Machine Learning Society, Madison, WI, 2008, pp. 272–279.
[28] B. D. Esry and C. H. Greene, *Validity of the shape-independent approximation for Bose-Einstein condensates*, Phys. Rev. A (3), 60 (1999), pp. 1451–1462.
[29] H. Fu, Y. Wang, and B. Gao, *Beyond the Fermi pseudopotential: A modified Gross-Pitaevskii equation*, Phys. Rev. A (3), 67 (2003), 053612.
[30] J. J. García-Ripoll, V. V. Konotop, B. Malomed, and V. M. Pérez-García, *A quasi-local Gross-Pitaevskii equation for attractive Bose-Einstein condensates*, Math. Comput. Simulation, 62 (2003), pp. 21–30.
[31] W. Kohn and L.J. Sham, *Self-consistent equations including exchange and correlation effects*, Phys. Rev. (2), 140 (1965), A1133.
[32] E. H. Lieb, R. Seiringer, and J. Yngvason, *Bosons in a trap: A rigorous derivation of the Gross-Pitaevskii energy functional*, Phys. Rev. A (3), 61 (2000), 043602.

[33] E. H. Lieb, R. Seiringer, J. Solovej, and J. Yngvason, *The mathematics of the Bose gas and its condensation*, Oberwolfach Semin., Birkhäuser, Basel, 2006.
[34] E. H. Lieb, B. Simon, *The Thomas-Fermi theory of atoms, molecules and solids*, Adv. Math., 23 (1977), pp. 22–116.
[35] P. Muruganandam and S. K. Adhikari, *Bose-Einstein condensation dynamics in three dimensions by the pseudospectral and finite-difference methods*, J. Phys. B, 36 (2003), pp. 2501–2513.
[36] Y. Nesterov, *A method of solving a convex programming problem with convergence rate* $O(1/k^2)$, Dokl. Akad. Nauk. SSSR, 269 (1983), pp. 543–547.
[37] P. M. Pardalos and N. Kovoor, *An algorithm for a singly constrained class of quadratic programs subject to upper and lower bounds*, Math. Program., 46 (1990), pp. 321–328.
[38] L. Pitaevskii and S. Stringari, *Bose-Einstein Condensation*, Internat. Ser. Monogr. Phys., Clarendon Press, Oxford, 2003.
[39] G. Roati, M. Zaccanti, C. D'Errico, J. Catani, M. Modugno, A. Simoni, M. Inguscio, and G. Modugno, ^{39}K *Bose-Einstein condensate with tunable interactions*, Phys. Rev. Lett., 99 (2007), 010403.
[40] X. Ruan, *A normalized gradient flow method with attractive-repulsive splitting for computing ground states of Bose-Einstein condensates with higher-order interaction*, J. Comput. Phys., 367 (2018), pp. 374–390.
[41] X. Ruan, *Mathematical Theory and Numerical Methods for Bose-Einstein Condensation with Higher Order Interactions*, Ph.D. thesis, National University of Singapore, Singapore, 2017.
[42] X. Ruan, Y. Cai, and W. Bao, *Mean-field regime and Thomas-Fermi approximations of trapped Bose-Einstein condensates with higher-order interactions in one and two dimensions*, J. Phys. B, 49 (2016), 125304.
[43] H. Veksler, S. Fishman, and W. Ketterle, *Simple model for interactions and corrections to the Gross-Pitaevskii equation*, Phys. Rev. A (3), 90 (2014), 023620.
[44] X. Wu, Z. Wen, and W. Bao, *A regularized Newton method for computing ground states of Bose–Einstein condensates*, J. Sci. Comput., 73 (2017), pp. 303–329.
[45] N. T. Zinner and M. Thøgersen, *Stability of a Bose-Einstein condensate with higher-order interactions near a Feshbach resonance*, Phys. Rev. A (3), 80 (2009), 023607.